

Neutrino inclusive inelastic scattering off nuclei

S. A. Kulagin

Institute for Nuclear Research, 117312 Moscow, Russia

R. Petti

*Department of Physics and Astronomy,
University of South Carolina, Columbia SC 29208, USA*

We present a detailed description of high-energy neutrino and antineutrino inelastic inclusive scattering off nuclei in terms of nuclear structure functions. In our approach we take into account a QCD description of the nucleon structure functions as well as a number of basic nuclear effects including nuclear shadowing, Fermi motion and binding, nuclear pion excess and off-shell correction to bound nucleon structure functions. These effects prove to be important in the studies of charged-lepton deep-inelastic scattering. We discuss similarities and dissimilarities in the calculation of nuclear effects for charged-lepton and neutrino scattering caused by nonconserved axial current in neutrino scattering. We examine the Adler and the Gross-Llewellyn-Smith sum rules for nuclear structure functions and find a remarkable cancellation between nuclear shadowing and off-shell corrections in these sum rules. We present calculations of differential cross sections for inclusive neutrino and antineutrino scattering in comparison with recent data on different target materials.

PACS numbers: 13.60.Hb, 25.30.Pt, 24.85.+p

I. INTRODUCTION

The interest in the study of neutrino interactions with nuclei at intermediate and high energy has grown considerably in recent years (see, e.g., [1]). New experimental results on neutrino cross-sections are also obtained for different nuclear targets [2, 3, 4]. The presence of an axial-vector component in the weak current and the quark flavor selection distinguish neutrino interactions from charged-lepton (CL) and hadron collisions. This feature makes the neutrino (ν) and antineutrino ($\bar{\nu}$) data a unique source of information on the nucleon and nuclear structure. The understanding of neutrino propagation in matter is also important for astrophysics, cosmology and even geology applications.

The use of heavy nuclear targets in neutrino experiments is motivated by the need to collect a statistically significant number of interactions. For this reason, the understanding of nuclear effects is of primary importance for a correct interpretation of experimental results and for the evaluation of the corresponding uncertainties. An example of such synergy is provided by the precision electroweak measurements from neutrino interactions. The role of nuclear corrections to neutrino structure functions has recently been emphasized [5] in the context of the anomalous measurement of the weak mixing angle ($\sin^2 \theta_W$) reported by the NuTeV collaboration [6].

An accurate account of nuclear effects is not only important in the determination of electroweak parameters in neutrino scattering experiments, but also for the understanding

of neutrino masses and mixing. The next generation experiments would imply precision measurements to disentangle small oscillation signals from neutrino and antineutrino interactions on nuclei. This in turn would require us to improve our knowledge of $\nu(\bar{\nu})$ -nucleus cross-sections in order to reduce systematic uncertainties.

The availability of high-intensity neutrino beams from the recent NuMI [7] and JPARC [8] facilities offers new opportunities for detailed studies of cross sections and nuclear effects in neutrino interactions. One such example is MINER ν A [9], a dedicated experiment at Fermilab which will collect data in few years. On a longer time scale, the construction of a neutrino factory [10] would then allow a further step forward, finally reaching the ultimate precision of the neutrino probe.

In this work we present a calculation of inelastic neutrino-nucleus structure functions (SF) and differential cross sections in a wide kinematical range of the Bjorken variable x and momentum transfer squared Q^2 . Our goal is to develop a quantitative model incorporating existing data, which would be useful in interpreting $\nu(\bar{\nu})$ experiments.

Scattering experiments with charged leptons show that even in the deep-inelastic scattering (DIS) region, for which the energy and momentum transfer are larger than the nucleon mass M , nuclear SF differ from a simple sum over bound nucleons and a significant nuclear effect is present even in the scaling regime (see, e.g., [11]). As evidenced by numerous studies (see [12, 13] and also [14]), the lepton-nucleus DIS is characterized by different mechanisms in different kinematical regions of the Bjorken variable x . In a recent paper [14] we studied the charged-lepton DIS off nuclear targets and developed a quantitative model for nuclear structure functions, taking into account major nuclear effects including nuclear shadowing, Fermi motion and binding, nuclear pion excess and off-shell correction to bound nucleon structure functions. This approach showed a very good agreement with data on the EMC effect for light and heavy nuclei for both the x and Q^2 dependence. In the present paper we extend this approach to neutrino-nucleus inelastic scattering.

Although nuclear scattering mechanisms for high-energy charged leptons and neutrinos are similar in many respects (especially in the impulse approximation), there are important differences due to the presence of the axial-vector current in neutrino interactions. The interference between the vector and the axial-vector currents introduces C -odd terms in neutrino cross sections, which are described by SF F_3 . In the calculation of nuclear corrections, we separate the contributions to different SF according to their C -parity. We examine in detail the dependence of nuclear effects on C -parity and show that it is particularly important in the nuclear shadowing region. Results are then used to predict nuclear structure functions for neutrino and antineutrino interactions, respectively.

In contrast to the electromagnetic current, the axial current is not conserved, and for this reason the neutrino structure functions in the region of low Q^2 and small x are rather different from those of electroproduction. In particular, the neutrino longitudinal SF F_L (as well as F_2) does not vanish at low Q^2 . Its value is determined by the divergence of the axial-vector current which is linked to the virtual pion cross-section (Adler relation [15]). We discuss the derivation of this relationship for structure functions and examine corrections to that. We also address the phenomenological implications of this relation in the description of low- Q^2 and low- x neutrino differential cross sections. The nuclear shadowing effect on the virtual pion cross section results in a significant suppression of the corresponding nuclear structure functions.

The paper is organized as follows. In Sec. II we introduce the general formalism of neutrino inclusive inelastic scattering, define the structure functions and present the differential

cross sections for charged-current (CC) and neutral-current (NC) neutrino scattering. In Sec. IIC we summarize our model of the nucleon SF in the region of high Q^2 ; in Sec. IID we deal with the low- Q^2 region and discuss the separation of the axial current contribution from the vector component. In Sec. III we discuss the nuclear effects in neutrino DIS. Particular attention is paid to the calculation of neutrino C -even and C -odd structure functions. In Sec. IIID and IIIE we examine the Adler and the Gross-Llewellyn-Smith sum rules for nuclear targets. In Sec. IV we present the results of numerical analysis of SF and differential cross sections for a number of nuclear targets and compare our predictions with the recent data [2, 3, 4].

II. GENERAL FORMALISM OF NEUTRINO INCLUSIVE SCATTERING

To leading order in the weak coupling constant, neutrino scattering is described by the standard one-boson exchange process. Neutrino interactions can be mediated by the charged W^\pm boson (*charged current* or CC) or by the neutral Z boson (*neutral current* or NC). In the Standard Model (SM) the leptonic and hadronic charged currents can be written as

$$j_\lambda^- = \bar{e}O_\lambda^L\nu_e + \bar{\mu}O_\lambda^L\nu_\mu, \quad (1a)$$

$$J_\lambda^- = \bar{d}'O_\lambda^L u + \bar{s}'O_\lambda^L c, \quad (1b)$$

where $O_\lambda^L = (1 - \gamma_5)\gamma_\lambda$, and $d' = d \cos \theta_C + s \sin \theta_C$, $s' = -d \sin \theta_C + s \cos \theta_C$ are the superpositions of d - and s -quark states and θ_C is a Cabibbo angle ($\sin^2 \theta_C \approx 0.05$). For simplicity, we neglect contributions from the third generation of quarks and leptons. The superscript L in Eqs.(1) indicates that only left doublets participate in the CC weak interaction.

The neutral current can be written as

$$j_\lambda^0 = \sum_\ell \bar{\ell}(g_V^\ell - g_A^\ell \gamma_5)\gamma_\lambda \ell, \quad (2a)$$

$$J_\lambda^0 = \sum_q \bar{q}(g_V^q - g_A^q \gamma_5)\gamma_\lambda q, \quad (2b)$$

where the sum is taken over all types of leptons ($\ell = e, \nu_e, \mu, \nu_\mu$) and quarks ($q = u, d, c, s$). The vector and axial charges of quarks and leptons in the SM in terms of the weak mixing angle θ_W can be found in, e.g., [16].

A. Charged-current neutrino scattering

We first consider the CC (anti)neutrino inelastic inclusive scattering. In inclusive scattering, the final hadronic state is not detected and the differential cross section can be written as (see, e.g., [16])

$$d^3\sigma_{\text{CC}} = \frac{2\pi G_F^2/(4\pi)^3}{(1 + Q^2/M_W^2)^2} L_{\mu\lambda} W_{\mu\lambda} \frac{d^3k'}{(p \cdot k)E'}, \quad (3)$$

where G_F is the Fermi weak coupling constant; M_W is the W -boson mass; p is the target four-momentum; $k = (E, \mathbf{k})$ and $k' = (E', \mathbf{k}')$ are four-momenta of the incoming and outgoing lepton, respectively; $q = k - k'$ is four-momentum transfer and $Q^2 = -q^2$. The tensors $L_{\mu\lambda}$ and $W_{\mu\lambda}$ describe the interaction of the W boson with leptons and hadrons, respectively. If

the polarization of the outgoing lepton is not detected, then the leptonic tensors for neutrino and antineutrino scattering are

$$L_{\mu\lambda}^{(\nu,\bar{\nu})} = 8 \left(k_\mu k'_\lambda + k_\lambda k'_\mu - k \cdot k' g_{\mu\lambda} \pm i \varepsilon_{\mu\lambda}(k, k') \right), \quad (4)$$

where the sign $+(-)$ corresponds to the neutrino (antineutrino). We use the contracted notation $\varepsilon_{\mu\lambda}(a, b) = \varepsilon_{\mu\lambda\alpha\beta} a^\alpha b^\beta$. The hadronic tensor $W_{\mu\lambda}$ is the sum of CC matrix elements over all possible final hadronic states. For the neutrino we have

$$W_{\mu\lambda}^{(\nu)}(p, q) = \frac{1}{4\pi} \sum_f (2\pi)^4 \delta(p + q - p_f) \langle p | J_\mu^{+\dagger}(0) | f \rangle \langle f | J_\lambda^+(0) | p \rangle, \quad (5)$$

where the current in the SM is given by Eq.(1b). The antineutrino tensor corresponds to the exchange of the W^- boson and is given by a similar equation with the current J_λ^+ replaced by J_λ^- .

For the scattering from an unpolarized target, there are five independent structure functions in the hadronic tensor (5) for either the neutrino or antineutrino (see, e.g., [16])

$$\begin{aligned} W_{\mu\lambda}(p, q) = & \left(\frac{q_\mu q_\lambda}{q^2} - g_{\mu\lambda} \right) F_1 + \left(p_\mu - q_\mu \frac{p \cdot q}{q^2} \right) \left(p_\lambda - q_\lambda \frac{p \cdot q}{q^2} \right) \frac{F_2}{p \cdot q} \\ & + i \varepsilon_{\mu\lambda}(p, q) \frac{F_3}{2p \cdot q} + \frac{q_\mu q_\lambda}{Q^2} F_4 + \frac{q_\mu p_\lambda + q_\lambda p_\mu}{p \cdot q} F_5. \end{aligned} \quad (6)$$

We use the normalization of states $\langle p | p' \rangle = 2E_{\mathbf{p}} (2\pi)^3 \delta(\mathbf{p} - \mathbf{p}')$ for both the bosons and fermions. In this normalization the hadronic tensor (5) and the structure functions are dimensionless. The terms with F_1 and F_2 are similar to those in charged-lepton scattering. They originate from vector-vector and axial-axial correlations in Eq.(5). The antisymmetric term (F_3) describes parity-violating vector-axial and axial-vector transitions. The terms F_4 and F_5 are present because of nonconservation of the axial current.

The neutrino and antineutrino structure functions are apparently different. We will also consider the sum and the difference of neutrino and antineutrino structure functions, which have definite C -parity

$$F_i^{\nu\pm\bar{\nu}} = F_i^\nu \pm F_i^{\bar{\nu}}, \quad (7)$$

Contracting the leptonic and hadronic tensors, we obtain the explicit form of the differential cross section in terms of the structure functions. Using the usual variables $x = Q^2/(2p \cdot q)$ and $y = p \cdot q/p \cdot k$ we have

$$\frac{d^2 \sigma_{\text{CC}}^{(\nu,\bar{\nu})}}{dx dy} = \frac{G_F^2(p \cdot k)/\pi}{(1 + Q^2/M_W^2)^2} \sum_{i=1}^5 Y_i F_i^{(\nu,\bar{\nu})}. \quad (8)$$

The kinematical factors Y_i read as follows

$$Y_1 = y^2 x \frac{Q'^2}{Q^2} \left(1 - \frac{m'^2}{2Q^2} \right), \quad (9a)$$

$$Y_2 = \left(1 - \frac{yQ'^2}{2Q^2} \right)^2 - \frac{y^2 Q'^2}{4Q^2} \left(1 + \frac{p^2 Q^2}{(p \cdot q)^2} \right), \quad (9b)$$

$$Y_3 = \pm xy \left(1 - \frac{yQ'^2}{2Q^2} \right), \quad (9c)$$

$$Y_4 = \frac{yQ'^2}{4Q^2} \frac{m'^2}{p \cdot k}, \quad (9d)$$

$$Y_5 = -\frac{m'^2}{p \cdot k}, \quad (9e)$$

where the sign $+(-)$ refers to neutrino (antineutrino) scattering, m' is the mass of the outgoing charged lepton and $Q'^2 = Q^2 + m'^2$. We keep the lepton mass terms for completeness. Although these terms are tiny in ν_e and ν_μ scattering, they are not negligible in ν_τ scattering. The contributions from the structure functions F_4 and F_5 to the neutrino production cross section are suppressed at high energy by a small ratio $m'^2/p \cdot k$.

The structure functions can be related to the virtual boson helicity cross sections by projecting Eq.(6) onto the states with definite polarizations of an intermediate vector boson [for simplicity, we suppress explicit notation for (anti)neutrino hadronic tensor]

$$W_h = e_h^{\mu*} W_{\mu\nu} e_h^\nu, \quad (10)$$

where e_h^μ is the polarization vector of the virtual boson in the helicity state h ($h = \pm 1$ corresponds to two transverse polarizations, and $h = 0$ to the longitudinal polarization). The relation between the helicity structure functions W_h and $F_{1,2,3}$ can be derived from Eq.(6) using an explicit form of polarization vectors and the orthogonality and normalization conditions for polarization vectors (see, e.g., [14, 16]). We have

$$W_{\pm 1} = F_1 \pm \gamma F_3, \quad (11a)$$

$$W_0 = \gamma^2 F_2 / (2x) - F_1. \quad (11b)$$

One concludes from Eqs.(11) that F_1 is the transverse structure function averaged over transverse polarizations and F_3 is determined by the right-left asymmetry in helicity structure functions $W_{+1} - W_{-1}$. Below, we also use $F_T = 2xF_1$, $F_L = 2xW_0$ and $R = F_L/F_T$.

B. Neutral-current neutrino scattering

The NC hadronic tensor is given by Eq.(5), in which the charged current must be replaced by the neutral current. The leptonic tensor in this case is given by Eq.(4) with the overall factor 1/2, reflecting the fact that the neutrino can only be left-polarized (and the antineutrino, right-polarized). As a result, the NC cross section has the overall factor 1/2 compared to Eq.(8),

$$\frac{d^2\sigma_{CC}^{(\nu,\bar{\nu})}}{dx dy} = \frac{G_F^2(p \cdot k)/(2\pi)}{(1 + Q^2/M_Z^2)^2} \sum_{i=1}^5 Y_i F_i^Z, \quad (12)$$

where M_Z is the mass of the Z boson and the kinematical factors Y_i are obtained from Eqs.(9) by taking the limit $m' \rightarrow 0$. Therefore, the structure functions F_4 and F_5 do not contribute to the NC cross section. We also comment that neutrino and antineutrino NC structure functions of the type i are identical, because the neutrino and antineutrino in NC scattering couple to the same hadronic current.

C. Neutrino structure functions at high Q^2

At high Q^2 , above the resonance region, the structure functions are usually described in QCD as a series in Q^{-2} on the basis of the operator product expansion of the correlator of the weak currents (twist expansion) [17]. The leading twist (LT) terms correspond to quasifree scattering off quarks corrected for gluon radiation effects. In this approximation the structure functions are given in terms of parton distributions or PDFs (see, e.g., [16, 18]). The PDFs are universal high-momentum transfer characteristics of the target. The PDFs have a nonperturbative origin and their dependence on the Bjorken variable x can not be calculated in perturbative QCD. However, the dependence of PDFs on momentum transfer is governed by the perturbation theory in strong coupling constant α_s at the scale Q^2 (DGLAP evolution equations [19]). Currently, the coefficient and the splitting functions, which determine the QCD evolution, are known up to two-loop approximation (NNLO approximation) [20, 21].

Along with the LT terms, the higher order Q^{-2} terms have to be taken into account (higher twists or HT). The HT terms can be of two different sources: (i) the kinematical target mass terms which can be approximately resummed and absorbed into the LT terms according to [22, 23] and (ii) the dynamical HT terms which are related to quark-gluon correlation effects. In summary, the structure function of type i can be written as a power series

$$F_i(x, Q^2) = F_i^{\text{TMC}}(x, Q^2) + H_i^{(4)}/Q^2 + \dots, \quad (13)$$

where F_i^{TMC} is the LT structure function corrected for the target mass effects and $H_i^{(t)}$ are the functions of x and Q^2 describing the strength of the HT terms of twist t . In this paper the target mass corrections are computed using the approach of Ref.[22]. In order to keep the correct threshold behaviour of structure functions for $x \rightarrow 1$, we expand F_i^{TMC} in a power series in Q^{-2} and keep the terms to the order Q^{-2} [14].

In the numerical analysis the LT structure functions are computed using both the PDFs and the coefficient functions to the NNLO approximation. We use the PDFs and HT of Ref.[24], obtained from a new fits optimized at low Q^2 and including additional data. It should be noted that unlike the PDFs the HT terms are not universal and generally depend on the type of the structure function i as well as on the type of interaction. In order to evaluate HT in neutrino DIS, we assume that the ratio H_i/F_i^{LT} is similar for CL and neutrino structure functions as a working hypothesis. That allows us to use the phenomenological HT terms extracted from the fits to CL DIS data. We also assume no HT terms for F_3 in the calculations of nuclear structure functions and differential cross sections presented in Sec. IV.

In the calculation of neutrino cross sections for the structure function F_5 we use the Albright–Jarlskog relation $2xF_5 = F_2$ [27]. Recently, it was argued that this relation survives QCD higher order corrections and the target mass corrections [28]. For F_4 we will use the relation $F_4 = F_2/(2x) - F_1$ which replaces the Albright–Jarlskog relation $F_4 = 0$ for massless quarks if the target mass corrections are taken into account [28].

D. Neutrino structure functions at low Q^2

We note that even for high-energy scattering in the fixed-target experiments the events with small Bjorken x typically have the values of Q^2 below 1 GeV^2 . In this Section we discuss

the vector- and the axial-current contributions to neutrino structure functions at low Q^2 and outline the model which will be used in our studies of neutrino differential cross sections. In this context it is useful to review the requirements which follow from conservation of the vector current and partial conservation of the axial current. It follows from Eqs. (10) and (5) that the structure functions F_T and F_L can be written as

$$F_{T,L} = \frac{\gamma}{\pi} Q^2 \sigma_{T,L}, \quad (14)$$

where $\sigma_{T(L)}$ refers to the total cross section induced by the transverse (longitudinal) component of the weak current J_λ ,

$$\sigma_{T,L} = \frac{1}{4j} \sum_f (2\pi)^4 \delta(p + q - p_f) |\langle p | e_{T,L} \cdot J(0) | f \rangle|^2, \quad (15)$$

where $j = ((p \cdot q)^2 - p^2 q^2)^{1/2}$ is the invariant flux of the virtual boson with four-momentum q on the target with four-momentum p (for the nucleon at rest $j = M|\mathbf{q}|$, with M the nucleon mass) and the sum is taken over all possible final states. The transverse cross section does not vanish in the limit $Q^2 \rightarrow 0$; therefore F_T vanishes as Q^2 in this limit. This holds for both the vector- and the axial-current contributions.

In the longitudinal channel the low- Q behavior of the vector- and axial-current parts are different. We first consider the contribution from the *vector current*. The conservation of the vector current (CVC) suggests $q_\mu W_{\mu\nu} = 0$ for the vector-current part of the hadronic tensor. From this condition we conclude that F_L^{VC} vanishes faster than F_T^{VC} at low Q^2 and $F_L^{\text{VC}}/F_T^{\text{VC}} \sim Q^2/q_0^2$, similar to the charged-lepton case.

In contrast to the vector current, the axial current is not conserved and, according to the hypothesis of partial conservation of the axial current (PCAC), its divergence is proportional to the pion field [15],

$$\partial A^\pm = f_\pi m_\pi^2 \varphi^\pm, \quad (16)$$

where m_π is the pion mass and $f_\pi = 0.93m_\pi$ is the pion decay constant and φ^\pm is the pion field in the corresponding charge state. The PCAC relation can be used to compute the axial current contribution to the longitudinal structure function F_L^{AC} in the region of low momentum transfer. In this context it is useful to explicitly separate the pion contribution to the axial current,

$$A_\mu = -f_\pi \partial_\mu \varphi + A'_\mu, \quad (17)$$

where the operator A' describes the contributions from heavy hadron states, i.e. the contributions from axial-vector meson states, $\rho\pi$ continuum, etc. It is important to notice that the pion derivative term does not contribute to the structure functions [29]. This is because the matrix elements of $\partial_\mu \varphi$ are proportional to the momentum transfer q_μ . These terms give a vanishing contribution when contracted with the boson polarization vectors because of the orthogonality condition $e_h \cdot q = 0$ for any helicity state h . Therefore, the axial-vector operator A_μ can be replaced by A'_μ everywhere in Eqs.(5). The PCAC relation for A' follows from Eq.(16):

$$\partial A'^\pm = f_\pi j_\pi^\pm, \quad (18)$$

where $j_\pi^\pm = (\partial^2 + m_\pi^2)\varphi^\pm$ is the pion current. In order to calculate F_L we separate the contribution of the axial current to the hadronic tensor (5), contract it with the polarization

vector e_0 and replace A with A' .¹ Using Eq.(18) we have

$$F_L^{\text{AC}} = \gamma^3 F_L^{\text{PCAC}} + 2\gamma^3 \frac{Q^2 f_\pi \sigma'_\pi}{\pi |\mathbf{q}|} + \tilde{F}_L^{\text{AC}}, \quad (19)$$

where $F_L^{\text{PCAC}} = f_\pi^2 \sigma_\pi / \pi$ and $\sigma_\pi = \sigma_\pi(s, Q^2)$ is the total cross section for scattering of a virtual pion with four-momentum q and the center-of-mass energy squared $s = (p + q)^2$

$$\sigma_\pi = \frac{1}{4j} \sum_f (2\pi)^4 \delta(p + q - p_f) |\langle p | j_\pi(0) | f \rangle|^2. \quad (20)$$

The flux j is defined in Eq.(15). Note also that π^+ cross section corresponds to the neutrino, and π^- to the antineutrino. The quantity σ'_π describes the interference between the divergence of the axial current and the operator A'_z in the hadronic tensor

$$\sigma'_\pi = \frac{1}{4j} \sum_{f'} (2\pi)^4 \delta(p + q - p_{f'}) \text{Im} \left(\langle p | j_\pi(0) | f' \rangle \langle f' | A'_z(0)^\dagger | p \rangle \right). \quad (21)$$

The last term in Eq.(19) is similar to F_L^{YC} and vanishes as Q^4 .

It follows from the relation $F_2 = (F_L + F_T)/\gamma^2$ and (19) that the structure function F_2 at low Q^2 is dominated by the F_L^{PCAC} term. The PCAC contribution to the neutrino cross sections at small values of Q^2 was experimentally tested in [30]. On the other hand, the PCAC term should vanish at high Q^2 . In order to interpolate between low and high Q^2 , we introduce a form factor $f_{\text{PCAC}}(Q^2)$

$$F_L^{\text{PCAC}} = \frac{f_\pi^2 \sigma_\pi}{\pi} f_{\text{PCAC}}(Q^2). \quad (22)$$

In the numerical analysis we assume a dipole form $f_{\text{PCAC}}(Q^2) = (1 + Q^2/M_{\text{PCAC}}^2)^{-2}$ with M_{PCAC} the mass scale controlling the PCAC mechanism. Since the pion pole does not contribute to the structure functions, the scale M_{PCAC} is not determined by the pion mass, but rather it is related to higher mass states like a_1 meson, $\rho\pi$ continuum etc. In the present paper we fix the numerical value of M_{PCAC} phenomenologically using low- Q^2 cross section data from the CHORUS experiment [4] (see Sec. IV D).

III. NUCLEAR ASPECTS OF NEUTRINO SCATTERING

In this Section we summarize the theoretical framework used in this paper to calculate the (anti)neutrino structure functions and cross sections for nuclear targets. A similar approach was recently applied in the studies of charged-lepton nuclear DIS [14]. In Sec. III A we review calculations of nuclear structure functions in the impulse approximation with off-shell corrections, in Sec. III B we discuss nuclear pion correction, in Sec. III C we deal with nuclear effects from coherent nuclear interactions of hadronic component of an intermediate boson, which are relevant at small x .

¹ To this end a covariant form of longitudinal vector $e_0^\mu = (q^\mu + p^\mu Q^2/p \cdot q)/Q$ is useful.

A. Incoherent scattering from bound nucleons

In the region of large Bjorken x the nuclear DIS is usually treated in impulse approximation, i.e. as an incoherent sum over bound protons and neutrons. In this approximation the nuclear structure functions can be written in terms of the convolution of the nuclear spectral function and off-shell nucleon structure functions. In the target rest frame we have (for a derivation and more details see [14, 32, 33, 34])

$$F_T^A(x, Q^2) = \sum_{\tau=p,n} \int [dp] \mathcal{P}^\tau(\varepsilon, \mathbf{p}) \left(1 + \frac{\gamma p_z}{M}\right) \left(F_T^\tau + \frac{2x'^2 \mathbf{p}_\perp^2}{Q^2} F_2^\tau\right), \quad (23a)$$

$$F_L^A(x, Q^2) = \sum_{\tau=p,n} \int [dp] \mathcal{P}^\tau(\varepsilon, \mathbf{p}) \left(1 + \frac{\gamma p_z}{M}\right) \left(F_L^\tau + \frac{4x'^2 \mathbf{p}_\perp^2}{Q^2} F_2^\tau\right), \quad (23b)$$

$$\gamma^2 F_2^A(x, Q^2) = \sum_{\tau=p,n} \int [dp] \mathcal{P}^\tau(\varepsilon, \mathbf{p}) \left(1 + \frac{\gamma p_z}{M}\right) \left(\gamma'^2 + \frac{6x'^2 \mathbf{p}_\perp^2}{Q^2}\right) F_2^\tau. \quad (23c)$$

$$xF_3^A(x, Q^2) = \sum_{\tau=p,n} \int [dp] \mathcal{P}^\tau(\varepsilon, \mathbf{p}) \left(1 + \frac{p_z}{\gamma M}\right) x' F_3^\tau. \quad (23d)$$

where the integration is taken over the four-momentum of the bound nucleon $p = (M + \varepsilon, \mathbf{p})$ and $[dp] = d\varepsilon d^3\mathbf{p}/(2\pi)^4$. The axis z is chosen such that $q = (q_0, \mathbf{0}_\perp, -|\mathbf{q}|)$, \mathbf{p}_\perp is the transverse nucleon momentum, and $\gamma = |\mathbf{q}|/q_0$. The energy and momentum distribution of bound nucleons is described by the proton (neutron) nuclear spectral function $\mathcal{P}^{p(n)}(\varepsilon, \mathbf{p})$ which is normalized to the proton (neutron) number in a nucleus. In the integrand $F_i^{p(n)}$ are the structure functions of bound proton (neutron), which depend on the Bjorken variable $x' = Q^2/(2p \cdot q)$, momentum transfer square Q^2 and generally on the nucleon invariant mass squared $p^2 = (M + \varepsilon)^2 - \mathbf{p}^2$. The relation between the F_T , F_L and F_2 of the off-shell nucleon is similar to (11), i.e. $\gamma'^2 F_2 = F_T + F_L$ with $\gamma'^2 = 1 + 4x'^2 p^2/Q^2$. Note that $\gamma' = \gamma$ for the vanishing momentum of the bound nucleon. It should be also noted that the transverse motion of the bound nucleon in the target causes the mixture of different structure functions in Eqs. (23a) and (23b) to order $\mathbf{p}_\perp^2/(M|\mathbf{q}|)$.

1. Isoscalar and isovector contributions

Since complex nuclei typically have different numbers of protons and neutrons, the nuclear structure functions generally have both the *isoscalar* and the *isovector* parts. In order to separate the isoscalar and isovector contributions in Eqs.(23), we write the isoscalar ($\mathcal{P}^{p+n} = \mathcal{P}^p + \mathcal{P}^n$) and isovector ($\mathcal{P}^{p-n} = \mathcal{P}^p - \mathcal{P}^n$) nuclear spectral functions as

$$\mathcal{P}^{p+n} = A\mathcal{P}_0, \quad (24a)$$

$$\mathcal{P}^{p-n} = (Z - N)\mathcal{P}_1, \quad (24b)$$

where the reduced spectral functions \mathcal{P}_0 and \mathcal{P}_1 are normalized to unity. Using Eq.(24) we explicitly write Eqs.(23) in terms of isoscalar and isovector contributions

$$F_i^A/A = \langle F_i^N \rangle_0 + \frac{\beta}{2} \langle F_i^{p-n} \rangle_1, \quad (25)$$

where $F_i^N = \frac{1}{2}(F_i^p + F_i^n)$, $F_i^{p-n} = F_i^p - F_i^n$ for the structure function of type i and the parameter $\beta = (Z - N)/A$ describes the excess of protons over neutrons in a nucleus. The quantities $\langle F \rangle_0$ and $\langle F \rangle_1$ are the contracted notations of the integration in Eqs.(23) with reduced spectral functions \mathcal{P}_0 and \mathcal{P}_1 , respectively. The model of \mathcal{P}_0 and \mathcal{P}_1 , which is used in numerical applications in this paper, is discussed in more detail in Ref.[14].

Equation (25) is generic and can be applied to any structure function. We now discuss in more detail the $\nu \pm \bar{\nu}$ combinations of neutrino structure functions with definite C -parity (see Eq.(7)). Let us first consider symmetric $\nu + \bar{\nu}$ combination. From Eq.(25) we have

$$F_i^{(\nu+\bar{\nu})A}/A = \left\langle F_i^{(\nu+\bar{\nu})N} \right\rangle_0 + (\beta/2) \left\langle F_i^{(\nu+\bar{\nu})(p-n)} \right\rangle_1 \quad (26)$$

for any type i of the structure function.

In the absence of heavy quark contributions we have $F_i^{(\nu+\bar{\nu})p} = F_i^{(\nu+\bar{\nu})n}$ because of the isospin symmetry. For this reason the isovector term in Eq.(26) should vanish. However, we should remark that the isospin relations for structure functions for neutrino CC scattering are violated by the mixing of different quark generations and the c -quark mass effect, even in the presence of exact isospin symmetry on the PDF level. This effect results in the nonzero difference $F_i^{(\nu+\bar{\nu})(p-n)} \propto \sin^2 \theta_C$ with θ_C the Cabbibo mixing angle. Since the parameter β is small, this effect is suppressed in Eq.(26) and, therefore, it is a good approximation to keep only the isoscalar term in Eq.(26).

Let us now discuss the $\nu - \bar{\nu}$ asymmetry in the nuclear structure functions. From Eq.(25) we have for the nuclear structure function of the type i

$$F_i^{(\nu-\bar{\nu})A}/A = \left\langle F_i^{(\nu-\bar{\nu})N} \right\rangle_0 + (\beta/2) \left\langle F_i^{(\nu-\bar{\nu})(p-n)} \right\rangle_1. \quad (27)$$

The application of this equation to F_2 and xF_3 requires somewhat more attention. We first consider $F_2^{\nu-\bar{\nu}}$ (a similar discussion also applies to F_T and F_L). This structure function is C -odd and dominated by the isovector quark distributions. In the absence of the Cabbibo mixing effect we have $F_2^{(\nu-\bar{\nu})p} = -F_2^{(\nu-\bar{\nu})n}$. It follows from this relation that the first term in the right side of Eq.(27) vanishes and the nuclear structure function is determined by the second (isovector) term. Nuclear effects in this case are illustrated in Fig. 1.

However, the isospin relations for structure functions are violated by the heavy quark effect and the Cabbibo mixing angle, as was discussed above. This effect generates a nonzero value of $F_2^{(\nu-\bar{\nu})N} \propto \sin^2 \theta_C$. Surprisingly, this effect should not be neglected in the analysis of nuclear corrections for $\nu - \bar{\nu}$ asymmetries even in the first approximation. This is because the isovector contribution in Eq.(27) is suppressed by the factor β and thus the relative effect of $F_2^{(\nu-\bar{\nu})N}$ is enhanced. This effect is further discussed in Sec. IV, where we present the results of numerical calculation of nuclear structure functions.

Let us discuss Eq.(27) in application to xF_3 . Note that $xF_3^{\nu-\bar{\nu}}$ is C even and includes the contribution from the light quarks, which determines the isovector nuclear correction in Eq.(27), and the s -quark contribution to the isoscalar part in Eq.(27). In fact, the difference $xF_3^{(\nu-\bar{\nu})N}$ is driven by the s -quark distribution [recall that in the parton model $xF_3^{(\nu-\bar{\nu})N} = x(s + \bar{s})$]. Because β is a small parameter, the relative contribution from the isoscalar term in Eq.(27) is enhanced and we conclude that the asymmetry $xF_3^{\nu-\bar{\nu}}$ in nuclei is dominated by the strange quark contribution.

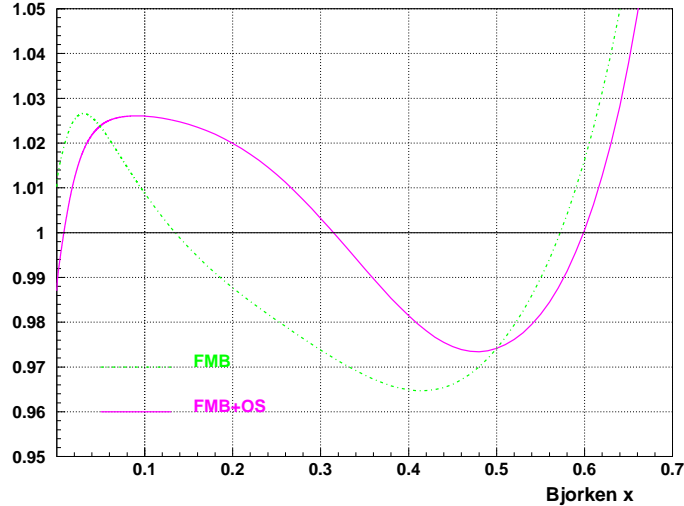


FIG. 1: The isovector nuclear effect $\langle F_2^{(\nu-\bar{\nu})p} \rangle_1 / F_2^{(\nu-\bar{\nu})p}$ calculated for ^{207}Pb at $Q^2 = 5 \text{ GeV}^2$ with and without off-shell correction using the isovector nuclear spectral function of Ref.[14]. The labels on the curves correspond to effects due to Fermi motion and nuclear binding (FMB) and off-shell correction (OS), which was calculated using Eq.(30).

2. Off-shell effects

The structure functions of the bound proton and neutron can differ from those of the free proton and neutron. In the approach discussed, this effect is related to analytical continuation of the structure functions to the off-shell region and the dependence on the nucleon invariant mass p^2 . One can separate the two sources of p^2 dependence: (i) the target mass correction leading to the terms of the order p^2/Q^2 and (ii) off-shell dependence of LT structure functions (or parton distributions). The off-shell dependence of the target mass effect is evaluated by the replacement $M^2 \rightarrow p^2$ in the expressions of Ref.[22]. In order to facilitate the discussion of the off-shell dependence of the LT structure functions, we note that characteristic momenta and energies of the bound nucleon are small compared to the nucleon mass, and the nucleon virtuality $v = (p^2 - M^2)/M^2$ is a small parameter. We then expand the LT structure functions in this parameter and keep the terms to the first order in v ,

$$F_2^{\text{LT}}(x, Q^2, p^2) = F_2^{\text{LT}}(x, Q^2) (1 + \delta f_2(x, Q^2) v), \quad (28)$$

$$\delta f_2 = \partial \ln F_2^{\text{LT}} / \partial \ln p^2, \quad (29)$$

where the first term on the right in Eq.(28) is the structure function of the on-mass-shell nucleon and the derivative is evaluated at $p^2 = M^2$. Similar expressions can be written for other structure functions.

The off-shell correction δf_2 was studied phenomenologically in [14] by analyzing the data on the ratios of structure functions of different nuclei (EMC effect). As a result it was found that δf_2 is independent of Q^2 with a good accuracy and can be parametrized as

$$\delta f_2 = C_N(x - x_1)(x - x_0)(1 + x_0 - x) \quad (30)$$

with the parameters extracted from the fit $C_N = 8.10 \pm 0.30(\text{stat.}) \pm 0.53(\text{syst.})$, $x_0 = 0.448 \pm 0.005(\text{stat.}) \pm 0.007(\text{syst.})$, and $x_1 = 0.05$.

Although the off-shell function (29) generally depends on the structure function type, it was assumed in Ref.[14] that the relative off-shell effect is common for all types of structure functions (or partons) and described by the off-shell function (30). It was tested that this assumption leads to fairly good cancellation between off-shell and nuclear shadowing effects in the normalization of the valence quark distribution. In this paper the off-shell function by Eq.(30) is applied in our calculations of nuclear (anti)neutrino structure functions. The interplay between off-shell (OS) and nuclear shadowing (NS) corrections in the DIS sum rules is further studied in Sec. III E and III D, where we discuss the Gross–Llewellyn-Smith and the Adler sum rules for nuclear targets.

B. Nuclear pion correction

The lepton scattering off the meson fields in nuclei gives rise to mesonic contribution to the nuclear structure functions (for a review see, e.g., [12, 13]). We note that because of binding the nucleons do not carry all of the nuclear light-cone momentum and the meson contribution is important for balancing the missing momentum. At high Q^2 the mesonic correction to nuclear structure functions can approximately be taken into account using the convolution model and the kinematics of the Bjorken limit neglecting power corrections. Then the pion correction to F_2^A can be written as

$$\delta_\pi F_2^A(x, Q^2) = \sum_\pi \int_x^1 dy f_{\pi/A}(y) F_2^\pi(x/y, Q^2), \quad (31)$$

where $f_{\pi/A}(y)$ is the distribution of nuclear pion excess² and F_2^π is the pion structure function and the sum is taken over different pion states $\pi = \pi^+, \pi^-, \pi^0$. Similar equations can be written for the pion correction to F_T and F_L with the same pion distribution function. We also note that the pion correction vanishes for F_3 . In the numerical analysis we also assume no off-shell effect in the virtual pion structure function, which would be the second order correction because (31) is a small correction by itself.

We apply Eq.(31) to $\nu \pm \bar{\nu}$ combinations of neutrino structure functions. It is convenient to separate the isoscalar and isovector contributions in the sum over pion states in Eq.(31). We also apply the isospin relations for the CC neutrino-pion SFs ($F_2^{(\nu+\bar{\nu})\pi}$ is isoscalar and independent of the pion charge state, and $F_2^{(\nu-\bar{\nu})\pi^+} = -F_2^{(\nu-\bar{\nu})\pi^-}$).³ We then have for the nuclear pion correction

$$\delta_\pi F_2^{(\nu+\bar{\nu})A}(x, Q^2) = \int_x^1 dy f_{\pi^0/A}^0(y) F_2^{(\nu+\bar{\nu})\pi^+}(x/y, Q^2), \quad (32a)$$

$$\delta_\pi F_2^{(\nu-\bar{\nu})A}(x, Q^2) = \int_x^1 dy f_{\pi^{\pm}/A}^1(y) F_2^{(\nu-\bar{\nu})\pi^+}(x/y, Q^2), \quad (32b)$$

where $f_{\pi^0/A}^0 = f_{\pi^+/A} + f_{\pi^-/A} + f_{\pi^0/A}$ and $f_{\pi^{\pm}/A}^1 = f_{\pi^+/A} - f_{\pi^-/A}$ are the isoscalar and the isovector pion distributions in a nucleus. In the applications discussed below, we neglect possible

² The contribution from the nucleon meson cloud should be subtracted since it is accounted for in the nucleon structure function.

³ We neglect here the violation of the isospin relations because of the Cabbibo mixing angle (see Sec. III A 1).

isovector contributions and use a model isoscalar pion distribution function, which obeys the constraints due to the nuclear light-cone momentum balance equation and equations of motion of the pion field in the nucleus (for more details see [14, 32]).

C. Coherent nuclear effects (shadowing and antishadowing)

At small x , at which the DIS longitudinal distance $L_I = 1/(Mx)$ is large compared to typical nuclear sizes, the nuclear DIS can be viewed as a two-step process in which the intermediate boson first fluctuates into a quark-antiquark pair (or hadronic configuration) which then scatters off the nucleus. As an average lifetime of this fluctuation is large (of order L_I), it can undergo multiple interactions with bound nucleons (for a recent review see, e.g., [12]). In this section we discuss nuclear effects in neutrino scattering associated with this mechanism and derive corrections for different SF types for ν and $\bar{\nu}$ interactions.

The structure functions at small x can be presented as a superposition of contributions from different hadronic states the virtual boson fluctuates to. For the helicity structure functions W_0 and W_{\pm} , as defined in Eq.(11), we have

$$W_h = \sum_i w_h(i) \sigma_h(i, s), \quad (33)$$

where σ_h is the total cross section of scattering of the hadronic state i with the given helicity $h = 0, \pm 1$ off the target nucleon (or nucleus) with the center-of-mass energy $s = Q^2(1/x - 1) + M^2$, and w_h describes the weight of the given hadronic state in the wave function of the intermediate boson.

We first consider the transverse structure functions with $h = \pm 1$ and approximate the sum over hadronic states in Eq.(33) by a factorized form [14]

$$W_h(x, Q^2) = w_h(x, Q^2) \bar{\sigma}_h(s), \quad (34)$$

where $\bar{\sigma}_h$ is an *effective* cross section averaged over hadronic configurations and w_h is the remaining normalization factor for the given helicity h . At low Q^2 and small x the effective cross section can be approximated by average vector meson cross section in the vector meson dominance model (VMD) (see, e.g., [37]). As Q^2 increases, the averaging in (34) involves the rising number of active hadronic states.

In the longitudinal case (W_0) we explicitly separate the PCAC term, Eq.(22), and assume that the rest, \tilde{F}_L , can be expressed by an equation similar to Eq.(34) with an effective longitudinal cross section.

In this paper we are concerned with the calculation of nuclear corrections to the structure functions and cross sections. In the following we will assume that the normalization factors w_h and the pion decay constant f_π are not affected by nuclear effects. Then for the transverse structure functions with $h = \pm 1$ the relative nuclear correction is determined by the corresponding correction to the effective cross section,

$$\delta\mathcal{R}_h = \frac{\delta W_h^A}{ZW_h^p + NW_h^n} = \frac{\delta\bar{\sigma}_h^A}{Z\bar{\sigma}_h^p + N\bar{\sigma}_h^n}, \quad (35)$$

where δW_h^A is the nuclear structure function of helicity h with the incoherent term subtracted, $\delta W_h^A = W_h^A - ZW_h^p - NW_h^n$, and a similar definition is used for $\delta\bar{\sigma}_h^A$. For the longitudinal structure function the corresponding relation to the cross section will be discussed in Sec.III C 4.

1. Multiple scattering corrections to helicity amplitudes

In order to calculate nuclear modifications of effective cross sections $\delta\sigma$ we apply the multiple scattering theory [35, 36]. Let $a^{p(n)}$ be the proton (neutron) effective scattering amplitude in forward direction. We will choose the normalization of the scattering amplitude such that the optical theorem reads $\text{Im } a(s) = \sigma(s)/2$ with σ the total cross section. For the following discussion it is convenient to write the forward scattering amplitude as

$$a = (i + \alpha)\sigma/2, \quad (36)$$

where $\alpha = \text{Re } a / \text{Im } a$. The nuclear scattering amplitude a^A can be written as

$$a^A = Z a^p + N a^n + \delta a^A, \quad (37)$$

where the first two terms on the right side are the incoherent contributions from bound protons and neutrons.⁴ The term δa^A is the multiple scattering correction (MS), which can be written as

$$\delta a^A = i \int_{z_1 < z_2} d^2\mathbf{b} dz_1 dz_2 e^{ik_L(z_1 - z_2)} a \cdot \rho(1) a \cdot \rho(2) e^{S(1,2,a)}, \quad (38)$$

$$S(1,2,a) = i \int_{z_1}^{z_2} dz' a \cdot \rho(\mathbf{b}, z'), \quad (39)$$

where $a \cdot \rho = a^p \rho^p + a^n \rho^n$ and $\rho^p(\rho^n)$ is the proton (neutron) nuclear density normalized to the proton (neutron) number and the integration is performed along the collision axis, which is chosen to be the z axis, and over the transverse positions of nucleons (impact parameter \mathbf{b}). We also use a contracted notation of the nucleon position on the collision axis $\rho(1) = \rho(\mathbf{b}, z_1)$, etc. The exponential factor in Eq.(38) accounts for multiple scattering effects (see, e.g., [37]) and for double scattering approximation e^S should be replaced by 1.

Amplitude (37) describes the scattering of virtual hadron configuration of the intermediate boson W^* off a nucleus. In intermediate states in the MS series one considers the scattering of on-mass-shell hadronic states, and for this reason there appears a nonzero longitudinal momentum transfer k_L . The quantity $L_c = 1/k_L$ is the longitudinal coherence length of this state. If m is the mass of intermediate state, then $k_L = Mx(1 + m^2/Q^2)$. Since the cross section in Eq.(34) refers to the effective intermediate hadronic state, we treat $m^2 = m_{\text{eff}}^2$ as a parameter.

Note that Eq.(38) was derived in the optical approximation assuming that the nuclear wave function factorizes into the product of the single particle wave functions. In this approximation possible effects of correlation between bound nucleons are neglected. We comment in this context that the correlations are relevant only if the coherence length L_c is comparable to the short-range repulsive part of the nucleon-nucleon force, which is about 0.5 Fm. However, this region is limited to relatively large x at which shadowing is a small correction (see discussion in Ref.[12]). The transverse momentum dependence of elastic scattering amplitudes was also neglected, that is justified by a small transverse size of the meson-nucleon amplitude compared to the nuclear radius.

⁴ The incoherent term is discussed in detail in Sec.III A together with nuclear binding, Fermi motion and off-shell effects. Here we focus on multiple scattering corrections.

We now apply Eq.(38) to describe nuclear effects generated by scattering of charged intermediate W^+ and W^- bosons. Let us first consider the contributions from the light (u and d) quarks. In this case the scattering amplitude obeys the requirements of the isospin symmetry and we can write the relations $a(W^\pm p) = a(W^\mp n) = a^0 \pm \frac{1}{2}a^1$, where a^0 and a^1 are the scattering amplitudes corresponding to the isoscalar and isovector nucleon configuration. Using these relations we have

$$a(W^\pm) \cdot \rho = (a^0 \pm \frac{1}{2}\beta a^1) \rho_A, \quad (40)$$

where $\rho_A = \rho_p + \rho_n$ is the (isoscalar) nucleon density and $\beta = (\rho_p - \rho_n)/\rho_A$ is the relative proton–neutron density asymmetry. In order to facilitate the discussion of isovector effects, we assume similar shapes of the proton and neutron densities. Then $\beta = (Z - N)/A$ is independent of the nucleon coordinate for nuclear interior. We also benefit from the fact that β is a small parameter for heavy nuclei, and expand the multiple scattering series (38) in β and keep the terms to first order in β . Then for the scattering of W^+ and W^- bosons we obtain

$$\delta a^A(W^\pm) = \mathcal{T}^A(a^0) \pm \frac{1}{2}\beta a^1 \mathcal{T}_1^A(a^0), \quad (41)$$

where

$$\mathcal{T}^A(a) = ia^2 \mathcal{C}_2^A(a), \quad (42a)$$

$$\mathcal{T}_1^A(a) = \frac{\partial}{\partial a} \mathcal{T}^A(a) = 2ia \mathcal{C}_2^A(a) - a^2 \mathcal{C}_3^A(a), \quad (42b)$$

and the quantities $\mathcal{C}_{2,3}^A$ incorporate the multiple scattering effects and read as follows:

$$\mathcal{C}_2^A(a) = \int_{z_1 < z_2} d^2 \mathbf{b} dz_1 dz_2 e^{ik_L(z_1 - z_2)} \rho_A(1) \rho_A(2) e^{S(1,2,a)}, \quad (43a)$$

$$\begin{aligned} \mathcal{C}_3^A(a) &= -i \frac{\partial}{\partial a} \mathcal{C}_2^A(a) = \\ &= \int_{z_1 < z_2 < z_3} d^2 \mathbf{b} dz_1 dz_2 dz_3 e^{ik_L(z_1 - z_3)} \rho_A(1) \rho_A(2) \rho_A(3) e^{S(1,3,a)}, \end{aligned} \quad (43b)$$

where the e^S factor is given by Eq.(39) with $a \cdot \rho$ replaced by $a\rho_A$. The rate of multiple scattering interactions is controlled by the value of the mean free path of hadronic fluctuation in a nucleus $l_f = (\rho_A \sigma)^{-1}$. If l_f is large compared with the nuclear radius (i.e. at low nucleon density or/and small effective cross section), then the e^S factor can be neglected and the coefficients \mathcal{C}_2^A and \mathcal{C}_3^A determine the double ($\sim \rho^2$) and the tripple ($\sim \rho^3$) scattering terms in the MS series. If l_f is small enough then the e^S factor should be taken into account.

We find from Eq.(41) that nuclear correction to the sum of W^+ and W^- scattering amplitudes is determined by the isoscalar amplitude a^0 , and the nuclear $W^+ - W^-$ asymmetry is proportional to βa^1 . Note that this asymmetry also depends on a^0 through multiple scattering effects. The implications to (anti)neutrino structure functions are discussed in the next section.

2. Dependence of nuclear effects on C -parity and isospin

Up to now the helicity dependence of nuclear correction was implicit. In this section we apply the results of Sec.III C 1 to the combinations of helicity amplitudes which correspond

to the structure functions of interest. Recall that F_T is given by the average $(W_{+1} + W_{-1})/2$, and F_3 is determined by the asymmetry $W_{+1} - W_{-1}$. We will assume that the helicity is conserved in the MS series so that Eq.(38) generalizes to scattering amplitude with given helicity a_h .⁵

The neutrino and antineutrino cross section correspond to the interaction of W^+ and W^- , respectively. It will be convenient to discuss the $\nu + \bar{\nu}$ average and $\nu - \bar{\nu}$ asymmetry since these combinations have definite C -parity. We use the notation $a_T^I = \frac{1}{2}(a_{+1}^I + a_{-1}^I)$ for the average transverse amplitude with the isospin $I = 0, 1$ and $a_\Delta^I = \frac{1}{2}(a_{+1}^I - a_{-1}^I)$ for the corresponding asymmetry. Note that the amplitudes a_T^0 and a_Δ^1 are C -even, while a_Δ^0 and a_T^1 are C -odd.⁶

Let us first consider the $\nu + \bar{\nu}$ sum of amplitudes and use Eq.(41) for helicity $h = +1$ and $h = -1$. In particular, we consider the helicity average (T) and asymmetry (Δ). Taking into account that $|a_\Delta^0| \ll |a_T^0|$ in the low- x region, we expand $\mathcal{T}^A(a_{\pm 1}^0)$ about a_T^0 to order $(a_\Delta^0)^2$ and obtain

$$\delta a_T^{(\nu+\bar{\nu})A} = 2 \mathcal{T}^A(a_T^0), \quad (44a)$$

$$\delta a_\Delta^{(\nu+\bar{\nu})A} = 2 a_\Delta^0 \mathcal{T}_1^A(a_T^0). \quad (44b)$$

Using these equations we compute ratios (35) for effective cross sections. We recall that in the Born approximation $a^{(\nu+\bar{\nu})A} = A 2a^0$ for either helicity state T or Δ and, therefore, the ratio Eq.(35) is $\delta \mathcal{R}^{\nu+\bar{\nu}} = \text{Im} \delta a^{(\nu+\bar{\nu})A} / (2A \text{Im} a^0)$. Using Eqs.(44) and (36) we obtain

$$\delta \mathcal{R}_T^{\nu+\bar{\nu}} = \sigma_T^0 \text{Re} [(i + \alpha_T^0)^2 \mathcal{C}_2^A(a_T^0)] / (2A), \quad (45a)$$

$$\delta \mathcal{R}_\Delta^{\nu+\bar{\nu}} = \text{Im} [(i + \alpha_\Delta^0) \mathcal{T}_1^A(a_T^0)] / A, \quad (45b)$$

where $\sigma_T^0 = 2 \text{Im} a_T^0$ is the effective cross section corresponding to the transverse isoscalar amplitude and $\alpha_h^I = \text{Re} a_h^I / \text{Im} a_h^I$. If the real part of the amplitude is small, then the MS correction is negative because of destructive interference of forward scattering amplitudes on the upstream nucleons that causes *shadowing* of virtual hadron interactions. On the other hand, if the real part is large then the interference in the double scattering term is constructive, which would lead to an *antishadowing* effect. It should be remarked that $\delta \mathcal{R}_\Delta^{\nu+\bar{\nu}}$ (the relative nuclear correction to the structure function $F_3^{\nu+\bar{\nu}}$) depends on the C -even cross section σ_T^0 . The result is also affected by the interference of the real parts of the amplitudes in the C -even and C -odd channels. If we only keep the double scattering term in Eqs. (45a) and (45b), we arrive at the following relation:

$$\delta \mathcal{R}_\Delta^{\nu+\bar{\nu}} / \delta \mathcal{R}_T^{\nu+\bar{\nu}} = 2 \frac{1 - \alpha_\Delta \alpha_T}{1 - \alpha_T^2}, \quad (46)$$

where α_T and α_Δ refer to $I = 0$ amplitudes. Factor 2 in Eq.(46) is a generic enhancement of the double scattering correction for the cross section asymmetry which has a combinatorial origin (in the context of F_3 it was discussed in [14, 38]). Ratio (46) can be further enhanced if the real parts of the C -odd and C -even amplitudes have different sign (this is indeed a realistic case as will be discussed below).

⁵ However, the helicity-flip processes can occur because of spin effects, which are not considered here.

⁶ The symmetry of the effective amplitude a_h^I becomes apparent if we recall the correspondence with the structure functions: $F_T^{\nu+\bar{\nu}} \sim \text{Im} a_T^0$, $F_T^{\nu-\bar{\nu}} \sim \text{Im} a_T^1$, $F_3^{\nu+\bar{\nu}} \sim \text{Im} a_\Delta^0$, $F_3^{\nu-\bar{\nu}} \sim \text{Im} a_\Delta^1$.

We now discuss the $\nu - \bar{\nu}$ asymmetry. We apply Eq.(41) to the amplitudes a_T and a_Δ . Similar to the $\nu + \bar{\nu}$ case, we expand $\mathcal{T}_1^A(a_{\pm 1}^0)$ about the average amplitude a_T^0 in a series in a_Δ^0 up to the first order term. We obtain

$$\delta a_T^{(\nu-\bar{\nu})A} = \beta \left[a_T^1 \mathcal{T}_1^A(a_T^0) + \frac{1}{4} a_\Delta^1 a_\Delta^0 \mathcal{T}_2^A(a_T^0) \right], \quad (47a)$$

$$\delta a_\Delta^{(\nu-\bar{\nu})A} = \beta \left[a_\Delta^1 \mathcal{T}_1^A(a_T^0) + a_T^1 a_\Delta^0 \mathcal{T}_2^A(a_T^0) \right], \quad (47b)$$

where $\mathcal{T}_2^A(a) = \frac{\partial}{\partial a} \mathcal{T}_1^A(a)$ [see Eqs.(42)]. Note that the first equation in (47) is C -odd and the second C -even. The quadratic terms $a^1 a^0$ in (47) produce a correction to the leading term of order $|a_\Delta^0/a_T^0|$. Taking into account the correspondence between effective amplitudes and the structure functions, we find that by order of magnitude $|a_\Delta^0/a_T^0|$ is the ratio of valence to sea quark distribution in the proton. This ratio is small in the region of small x ($x \ll 0.1$), where coherent nuclear effects are most important. For this reason in the following discussion we keep only the first term in the right side of (47). In this approximation the structure of Eqs.(47) is similar to that of Eq.(44b).

Using Eqs.(47) we calculate the relative corrections to the cross sections. For this purpose we recall that in the Born approximation $a^{(\nu-\bar{\nu})A} = (Z - N)a^1$ for either helicity state T or Δ . Then the ratio $\delta\mathcal{R}^{\nu-\bar{\nu}} = \text{Im} \delta a^{(\nu-\bar{\nu})A} / [(Z - N) \text{Im} a^1]$ can be written as

$$\delta\mathcal{R}_{T,\Delta}^{\nu-\bar{\nu}} = \text{Im} \left[(i + \alpha_{T,\Delta}^1) \mathcal{T}_1^A(a_T^0) \right] / A, \quad (48)$$

where α_T^1 and α_Δ^1 are the Re / Im ratios for the amplitudes a_T^1 and a_Δ^1 , respectively.

Note also that in terms of (I, C) classification $\delta\mathcal{R}_T^{\nu+\bar{\nu}} = \delta\mathcal{R}^{(0,+)}$, $\delta\mathcal{R}_\Delta^{\nu+\bar{\nu}} = \delta\mathcal{R}^{(0,-)}$, $\delta\mathcal{R}_T^{\nu-\bar{\nu}} = \delta\mathcal{R}^{(1,-)}$, and $\delta\mathcal{R}_\Delta^{\nu-\bar{\nu}} = \delta\mathcal{R}^{(1,+)}$. Figure 2 illustrates the x dependence of the ratios $\delta\mathcal{R}^{(I,C)}$ for different isospin and C -parity states.

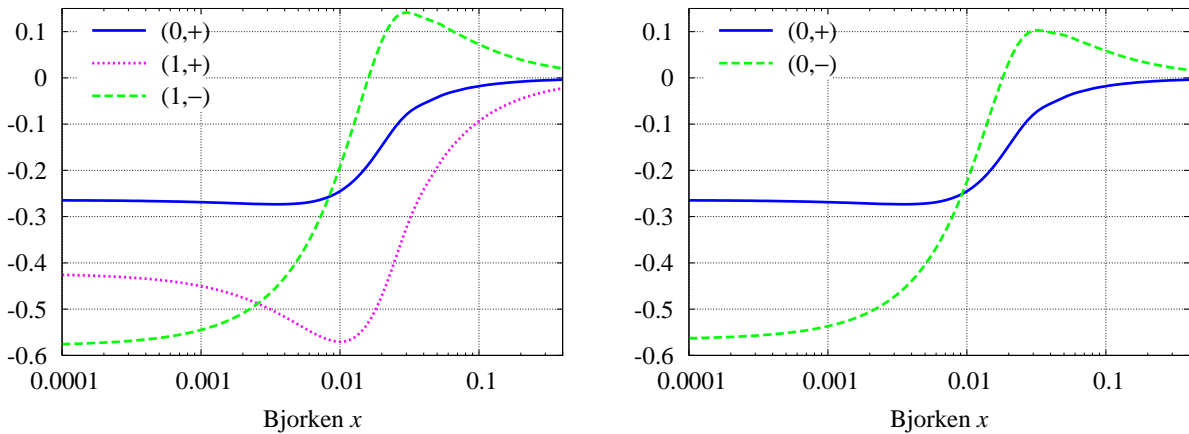


FIG. 2: The ratio $\delta\mathcal{R}^{(I,C)}$ calculated for different isospin and C -parity scattering states for ^{207}Pb at $Q^2 = 1 \text{ GeV}^2$ using the parameters of the scattering amplitudes from Sec. III C 5. The labels on the curves mark the values of the isospin I and C -parity, (I, C) .

3. Coherent nuclear correction to F_T and F_3

We now apply these results to neutrino structure functions. We recall that the discussion given above applies to the u - and d -quark contribution and make use of the isospin symmetry relations for the effective amplitude. In order to take into account the strange quark

contribution, we explicitly separate the light-quark (u and d) and the s -quark contributions to neutrino structure functions $i = T, 3$

$$F_i^{\nu+\bar{\nu}} = F_i^{(\nu+\bar{\nu})(0)} + F_i^{(\nu+\bar{\nu})(s)}, \quad (49a)$$

$$F_i^{\nu-\bar{\nu}} = F_i^{(\nu-\bar{\nu})(1)} + F_i^{(\nu-\bar{\nu})(s)}, \quad (49b)$$

where the superscripts indicate the contribution from the light quarks with total isospin 0 or 1, or the s -quark contribution. Although this separation is quite general, we illustrate the terms in Eqs.(49) in the parton model. For the transverse structure function we have $F_T^{(\nu+\bar{\nu})(0)} = x(u+d+\bar{u}+\bar{d})$, $F_T^{(\nu-\bar{\nu})(1)} = x(d-u+\bar{u}-\bar{d})$. The s -quark contribution is relevant for the C -even $F_T^{(\nu+\bar{\nu})(s)} = x(s+\bar{s})$. The C -odd $F_T^{(\nu-\bar{\nu})(s)}$ is proportional to $s-\bar{s}$ and can be neglected. Similarly, for $x F_3$ we have $x F_3^{(\nu+\bar{\nu})(0)} = x(u+d-\bar{u}-\bar{d})$, $x F_3^{(\nu-\bar{\nu})(1)} = x(d-u-\bar{u}+\bar{d})$, and $x F_3^{(\nu-\bar{\nu})(s)} = x(s+\bar{s})$. The C -odd $x F_3^{(\nu+\bar{\nu})(s)}$ is similar to $F_T^{(\nu-\bar{\nu})(s)}$ and can be neglected.

In general, the s -quark terms should be corrected differently from those of light quarks. Taking into account Eqs.(49) we have for coherent nuclear correction to the structure functions F_T and $x F_3$ per one nucleon

$$\delta F_T^{(\nu+\bar{\nu})A} = \delta \mathcal{R}^{(0,+)} F_T^{(\nu+\bar{\nu})(0)} + \delta \mathcal{R}^{(s,+)} F_T^{(\nu+\bar{\nu})(s)}, \quad (50a)$$

$$\delta F_3^{(\nu+\bar{\nu})A} = \delta \mathcal{R}^{(0,-)} F_3^{(\nu+\bar{\nu})(0)}, \quad (50b)$$

$$\delta F_T^{(\nu-\bar{\nu})A} = \beta \delta \mathcal{R}^{(1,-)} F_T^{(\nu-\bar{\nu})(1)}, \quad (50c)$$

$$\delta F_3^{(\nu-\bar{\nu})A} = \beta \delta \mathcal{R}^{(1,+)} F_3^{(\nu-\bar{\nu})(1)} + \delta \mathcal{R}^{(s,+)} F_3^{(\nu-\bar{\nu})(s)}, \quad (50d)$$

where the structure functions in the right side should be taken for the free proton and the ratios $\delta \mathcal{R}$ are given by Eqs. (45) and (48). Note that the s -quark contribution in Eq.(50d) is isoscalar and for this reason it is not suppressed by the factor β . From Eqs.(50) we derive coherent nuclear corrections to the (anti)neutrino structure functions. We define the ratio $\delta \mathcal{R}_i^{\nu}(A/N) = \delta F_i^{\nu A} / \delta F_i^{\nu N}$ describing the nuclear correction of the neutrino structure function of type i in the units of the isoscalar nucleon structure function $F_i^{\nu N} = (F_i^{\nu p} + F_i^{\nu n})/2$ [and similar definitions for the antineutrino ratio $\delta \mathcal{R}_i^{\bar{\nu}}(A/N)$]. We have

$$\delta \mathcal{R}_T^{\nu(\bar{\nu})}(A/N) = \delta \mathcal{R}^{(0,+)} \pm \beta \delta \mathcal{R}^{(1,-)} \frac{F_T^{(\nu-\bar{\nu})(1)}}{2 F_T^{\nu(\bar{\nu})N}} + (\delta \mathcal{R}^{(s,+)} - \delta \mathcal{R}^{(0,+)}) \frac{F_T^{(\nu+\bar{\nu})(s)}}{2 F_T^{\nu(\bar{\nu})N}}, \quad (51a)$$

$$\delta \mathcal{R}_3^{\nu(\bar{\nu})}(A/N) = \delta \mathcal{R}^{(0,-)} \pm \beta \delta \mathcal{R}^{(1,+)} \frac{F_3^{(\nu-\bar{\nu})(1)}}{2 F_3^{\nu(\bar{\nu})N}} \pm (\delta \mathcal{R}^{(s,+)} - \delta \mathcal{R}^{(0,-)}) \frac{F_3^{(\nu-\bar{\nu})(s)}}{2 F_3^{\nu(\bar{\nu})N}}, \quad (51b)$$

where the sign $+(-)$ corresponds to neutrino (antineutrino). In numerical applications in Sec. IV we will assume similar nuclear effects for $I = 0$ light quarks and the s -quark, $\delta \mathcal{R}^{(s,+)} = \delta \mathcal{R}^{(0,+)}$.

4. Coherent nuclear corrections to F_L and F_2

We now discuss coherent nuclear corrections to the longitudinal structure function. Nuclear modification of the PCAC term is driven by the corresponding correction to the virtual pion cross section, and we have $\delta F_L^{\text{PCAC}} / F_L^{\text{PCAC}} = \delta \sigma_{\pi A} / (A \sigma_{\pi N}) = \delta \mathcal{R}_{\pi}(A/N)$. The nuclear

correction to the pion cross section can be analyzed along the lines discussed in Sec. III C 1. We consider the isoscalar πN scattering amplitude $a_\pi^0 = (a_{\pi^+p} + a_{\pi^-p})/2$ and the isovector asymmetry $a_\pi^1 = a_{\pi^+p} - a_{\pi^-p}$. Nuclear corrections to these amplitudes are given by equations similar to (45a) and (48), and we have

$$\delta\mathcal{R}_\pi^0 = \sigma_\pi^0 \operatorname{Re} [(i + \alpha_\pi^0)^2 \mathcal{C}_2^A(a_\pi^0)] / (2A), \quad (52a)$$

$$\delta\mathcal{R}_\pi^1 = \operatorname{Im} [(i + \alpha_\pi^1) \mathcal{T}_1^A(a_\pi^0)] / A, \quad (52b)$$

where σ_π^0 is the πN cross section in the isoscalar state and $\alpha_\pi = \operatorname{Re} a_\pi / \operatorname{Im} a_\pi$ for the pion amplitude in the corresponding isospin state. In numerical applications we calculate $\delta\mathcal{R}_\pi$ using πN scattering amplitude of [31] (see Appendix A). Since the PCAC relation involves the cross section of the virtual pion with four-momentum q , the longitudinal momentum transfer in Eq.(38) is $k_L^\pi = Mx(1 + m_\pi^2/Q^2)$.

The ratios $\delta\mathcal{R}_\pi$ for the cross sections of π^+ and π^- mesons can be readily obtained from Eqs.(52), and we have

$$\delta\mathcal{R}_{\pi^\pm} = \delta\mathcal{R}_\pi^0 \pm (\beta\delta\mathcal{R}_\pi^1 - \delta\mathcal{R}_\pi^0) \frac{(\sigma_{\pi^+} - \sigma_{\pi^-})}{2\sigma_{\pi^\pm}}, \quad (53)$$

where the sign $+(-)$ corresponds to $\pi^+(\pi^-)$ scattering.

The nuclear corrections to the structure function \tilde{F}_L , which include the vector-current contribution and non-PCAC terms of the axial current, can be treated similarly to the transverse structure function F_T . In particular, we assume that the relative correction to \tilde{F}_L is determined by the effective cross section in the longitudinal state and $\delta\tilde{\mathcal{R}}_L = \delta\tilde{F}_L^A / \tilde{F}_L = \delta\bar{\sigma}_L^A / \bar{\sigma}_L$. Taking into account both contributions, we have for the relative nuclear correction to F_L

$$\delta\mathcal{R}_L(A/N) = r^{\text{PCAC}} \delta\mathcal{R}_\pi(A/N) + (1 - r^{\text{PCAC}}) \delta\tilde{\mathcal{R}}_L(A/N), \quad (54)$$

where $r^{\text{PCAC}} = \gamma^3 F_L^{\text{PCAC}} / F_L$ should be computed for the isoscalar nucleon.

Nuclear correction to F_2 can then be calculated in terms of the corresponding corrections for F_L and F_T using relation (11). We have for the relative correction

$$\delta\mathcal{R}_2(A/N) = \frac{\delta\mathcal{R}_T^A + R \delta\mathcal{R}_L^A}{1 + R}, \quad (55)$$

where $R = F_L/F_T$, and F_L and F_T are the structure functions of the isoscalar nucleon.

5. Effective scattering amplitude and cross section

We now discuss the model of the effective scattering amplitude for different isospin and helicity states a_h^I which is used in our calculations. This amplitude determines the rate of nuclear multiple scattering corrections as discussed above. In Ref.[14] the C -even amplitude a_T^0 was studied phenomenologically using charged-lepton data on the ratios $F_2^A/F_2^{A'}$, and it was shown that a good description of data for a wide region of nuclear targets can be achieved using a constant α_T^0 and the effective cross section parametrized as

$$\bar{\sigma}_T = \sigma_0 / (1 + Q^2/Q_0^2). \quad (56)$$

The values of the parameters were fixed to $\sigma_0 = 27$ mb and $\alpha_T = -0.2$ in order to reproduce the low- Q^2 limit [37]. The scale parameter Q_0^2 , which describes transition to high Q^2 , was determined to be $Q_0^2 = 1.43 \pm 0.06(\text{stat}) \pm 0.20(\text{syst}) \text{ GeV}^2$.

In this paper we test the hypothesis that the C -even effective amplitude a_T^0 also applies to the (anti)neutrino scattering and determine $F_T^{\nu+\bar{\nu}}$. The other amplitudes (a_Δ^0 , a_T^1 , a_Δ^1) are not directly constrained by the CL DIS data. These quantities determine nuclear corrections to different combinations of neutrino and antineutrino structure functions as discussed in Sec. III C. It is important to note that only Re/Im ratios of these amplitudes are relevant for the calculation of nuclear corrections to the (anti)neutrino structure functions. In order to evaluate Re/Im ratios we apply the Regge pole approach, which proved to be very useful in analyses of high-energy hadron scattering (see, e.g., [39]), and approximate the scattering amplitudes by a single Regge pole with proper quantum numbers. We recall that Re/Im of the Regge pole amplitude in forward direction is determined by its intercept $\alpha_R(0)$ and the signature (the latter corresponds to C parity of the scattering amplitude) $\text{Re/Im} = -(C + \cos \pi\alpha_R(0))/\sin \pi\alpha_R(0)$. The Regge poles of ω , ρ , and A_2 mesons have appropriate quantum numbers (see Table I; as known from hadron scattering phenomenology [39] these Regge trajectories have an intercept close to 0.5). In our calculations of (anti)neutrino nuclear scattering discussed below, we use the amplitude a_T^0 derived from the analysis of charged-lepton nuclear data [14]. The Re/Im ratio for the amplitudes a_Δ^0 and a_T^1 are fixed from the studies of the Adler and the Gross–Llewellyn-Smith sum rules for nuclear structure functions (see Sec. III D and III E).

Amplitude	a_Δ^0	a_T^1	a_Δ^1
Regge pole (I^C)	$\omega(0^-)$	$\rho(1^-)$	$A_2(1^+)$
Re/Im	1.15 (1)	1.35 (1)	(-1)

TABLE I: Regge poles contributing to the effective amplitude in different isospin and C parity states. Shown are the values of the Re/Im ratio extracted from analysis of nuclear corrections to the Adler and the GLS sum rules (see Sec. III D and III E) and those calculated with the intercept $\alpha_R(0) = 0.5$ common for all Regge poles (in parenthesis).

The effective cross section $\bar{\sigma}_L$ for longitudinally polarized intermediate states, which describes nuclear corrections to \tilde{F}_L (see Sec. III C 4), includes contributions from the vector and the axial currents. We separate the PCAC contribution to F_L , Eq.(22), and treat it explicitly as described in Sec. II D and III C 4. The remaining part \tilde{F}_L is described by the vector and non-PCAC terms of the axial current. We assume that \tilde{F}_L is similar to F_L in CL scattering. In order to quantitatively evaluate $\bar{\sigma}_L$, we assume the relation $\bar{\sigma}_L/\bar{\sigma}_T = \tilde{F}_L/F_T = \tilde{R}$, which allows to calculate $\bar{\sigma}_L$ in terms of $\bar{\sigma}_T$ and \tilde{R} . This relation follows from (34) if the normalization factors are independent of helicity. This can be justified in the VMD model at low Q^2 [14] and we also apply this relation to the region of high Q^2 . For $Q^2 > 1 \text{ GeV}^2$ for \tilde{R} we use the ratio F_L/F_T calculated using phenomenological PDFs and HT terms of [24]. In order to obtain \tilde{R} at $Q^2 < 1 \text{ GeV}^2$ we extrapolate from large Q^2 , assuming $\tilde{R} \propto Q^2$ at $Q^2 \rightarrow 0$.

It should be also commented that the nuclear MS effect in the transition region of x from 0.01 to 0.1 and Q^2 below 1 GeV^2 is affected by the value of the mass of effective intermediate state m_{eff} through k_L [see Eq.(38)]. In our studies of the charged-lepton data we used the value $m_{\text{eff}} = 0.9M$ which nicely fits the shadowing data. We also apply this parameter in the calculation of the vector-current contribution in neutrino scattering. Apparently, for

the axial current this parameter could be different because of different set of intermediate states. In order to account for this effect we use a simple ansatz of rescaling m_{eff} with the ratio of a_1 - and ρ -meson masses, $m_{\text{eff}}m_{a_1}/m_\rho$. Figure 3 illustrates the dependence of the ratios $\delta\mathcal{R}^{(0,+)}$ and $\delta\mathcal{R}^{(0,-)}$ on the parameter m_{eff} . Note that this dependence is noticeable for the transition region of $0.01 < x < 0.1$ and for low Q^2 .

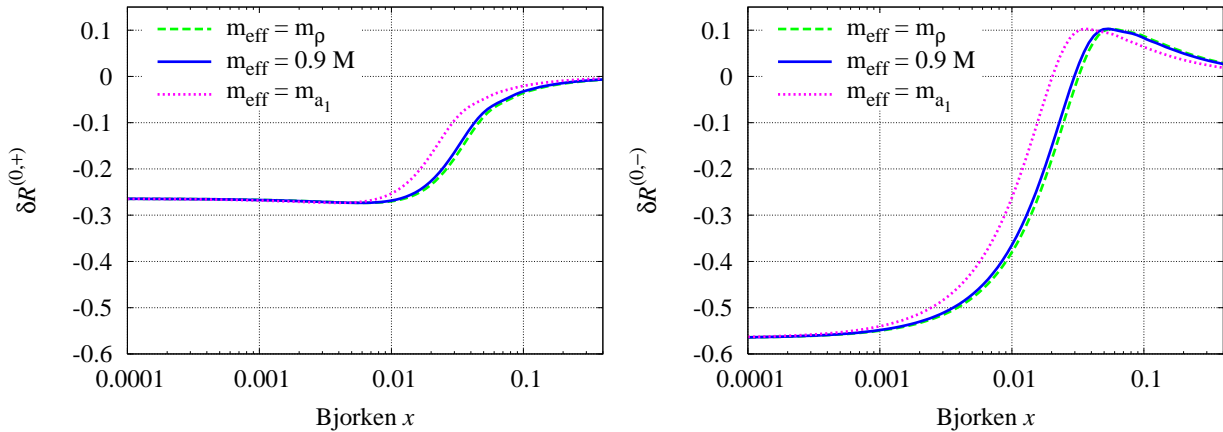


FIG. 3: The ratios $\delta\mathcal{R}^{(0,+)}$ and $\delta\mathcal{R}^{(0,-)}$ calculated for ^{207}Pb at $Q^2 = 1 \text{ GeV}^2$ using the scattering amplitudes from Sec. III C 5 and different values of the parameter m_{eff} .

D. The Adler sum rule for nuclei

The Adler sum rule relates the integrated difference of the isovector combination $F_2^{\nu-\bar{\nu}}$ to the isospin of the target:

$$S_A = \int_0^{M_A/M} dx F_2^{\nu-\bar{\nu}}(x, Q^2)/(2x) = 2 I_z, \quad (57)$$

where the upper integration limit, the ratio of the nuclear and the nucleon masses M_A/M , is the kinematical maximum of the Bjorken variable $x = Q^2/(2Mq_0)$ for the nuclear target, and I_z is the projection of the target isospin vector on the quantization axis (z axis). For the proton $S_A^p = 1$, and for the neutron $S_A^n = -1$. In the quark parton model the Adler sum is the difference between the number of valence u and d quarks of the target. The Adler sum rule survives the strong interaction effects because of CVC. However, in the derivation of the Adler sum rule the effects of nonconservation of the axial current as well as the Cabibbo mixing angle are neglected (for more detail see, e.g., [16]).

For an isoscalar nucleus the Adler sum rule is trivial since the integrand in Eq.(57) vanishes. For a generic nucleus of Z protons and N neutrons the Adler sum rule reads (we consider the nuclear structure functions per one nucleon)

$$S_A^A = (Z - N)/A = \beta. \quad (58)$$

We now discuss in turn the contributions to S_A from different nuclear effects. Let us first consider the Fermi motion and binding (FMB) corrections to $F_2^{\nu-\bar{\nu}}$ from Eq.(27). We will consider the kinematics of high Q^2 and neglect power Q^{-2} terms in nuclear convolution. By

performing the direct integration by x of Eq.(27) in the case of F_2 and using the isospin relations for the proton and neutron structure functions, we obtain

$$S_A = \beta \int \frac{dx}{2x} \left\langle F_2^{(\bar{\nu}-\nu)p} \right\rangle_1 = \beta + \delta S_A^{\text{OS}}, \quad (59a)$$

$$\delta S_A^{\text{OS}} = \beta \int_0^1 \frac{dx}{2x} F_2^{(\bar{\nu}-\nu)p}(x, Q^2) \delta f_2(x) \langle v \rangle_1, \quad (59b)$$

where $\langle v \rangle_1 = \langle p^2 - M^2 \rangle_1 / M^2$ is the nucleon virtuality averaged with the isovector spectral function \mathcal{P}_1 . Note that the FMB correction cancels out in (59a) in the impulse approximation. The integral in Eq.(59b) describes the variation of the Adler sum for the off-shell proton [the structure functions in (59b) should be taken for the on-shell proton]. In the derivation of the OS correction to the Adler sum rule (59b) we assume a universal off-shell function δf_2 , i.e. common for proton and neutron and independent from the probe (neutrino or antineutrino).

The nuclear pion correction to the Adler sum rule is computed using Eq.(32b). We have

$$\delta S_A^\pi = 2 (n_{\pi^+/A} - n_{\pi^-/A}), \quad (60)$$

where $n_{\pi/A} = \int dy f_{\pi/A}(y)$ is the average nuclear pion excess of the given pion type. These quantities also determine the pion excess correction to the total nuclear charge. From the charge conservation we have $n_{\pi^+/A} = n_{\pi^-/A}$ and, therefore, $\delta S_A^\pi = 0$.

The nuclear shadowing effect in the Adler sum can be computed using the results of Sec. III C. We integrate the shadowing correction $\delta F_2^{\bar{\nu}-\nu}$ [see Eqs.(50)] and obtain

$$\delta S_A^{\text{NS}} = \beta \int_0^1 \frac{dx}{2x} F_2^{(\bar{\nu}-\nu)p}(x, Q^2) \delta \mathcal{R}_2^{(1,-)}, \quad (61)$$

where $\delta \mathcal{R}_2^{(1,-)}$ is given in terms of $\delta \mathcal{R}_T^{(1,-)}$ and $\delta \mathcal{R}_L^{(1,-)}$ by Eq.(55).

It follows from Eqs. (58) and (59a) that the total nuclear correction to the Adler sum rule should vanish. This requirement provides an important constraint on the isovector part of nuclear structure functions. We verify that our approach is consistent with the Adler sum rule and explicitly calculate the OS and NS corrections as a function of Q^2 using the off-shell function δf_2 by Eq.(30) and effective cross section (56) derived from analysis of nuclear DIS with charged leptons [14]. It should be remarked that the quantity $\delta \mathcal{R}_T^{(1,-)}$ is also determined by α_T^1 , the Re / Im ratio of the isospin 1 transverse effective amplitude [see Eq.(48)]. This quantity is not constrained by charged-lepton data. We assume α_T^1 to be energy- and Q^2 -independent. In order to constrain this parameter we apply the requirement of minimization of the total nuclear correction to the Adler sum rule $\delta S_A = \delta S_A^{\text{OS}} + \delta S_A^{\text{NS}}$. In particular, we start from $\alpha_T^1 = 1$, as suggested by simple Regge arguments in Sec. III C 5, and try to adjust this parameter in order to minimize δS_A for all Q^2 . We found that $\alpha_T^1 = 1.35$ provides a good cancellation between the OS and NS corrections (see Fig. 4).

We also remark that phenomenological cross section (56) should be applied in the limited region of Q^2 . This is because this quantity was constrained by nuclear shadowing data in DIS which are limited to the region $Q^2 < 20 \text{ GeV}^2$ [14]. In order to evaluate the effective cross section at higher values of Q^2 we take the requirement $\delta S_A = 0$ as equation on the cross section and solve it numerically. The result of calculation for iron is shown in Fig. 4. Also shown is the effective cross section obtained from a similar calculation for the normalization

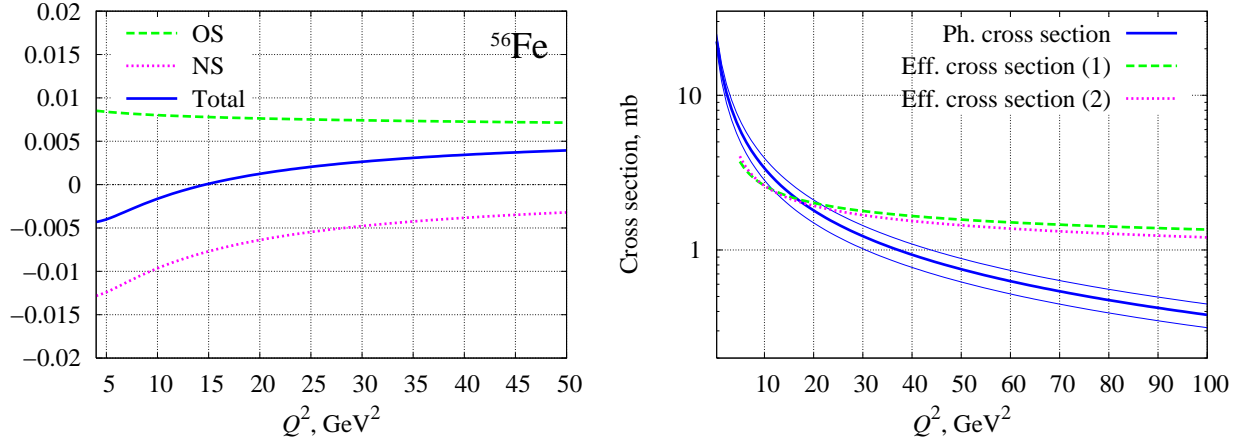


FIG. 4: Relative off-shell (OS), nuclear shadowing (NS) and total nuclear correction to the Adler sum rule calculated for iron (left panel). The right panel shows phenomenological cross section by Eq.(56) with the error band and effective cross section computed by requiring exact cancellation between OS and NS effects in nuclear Adler sum rule (1) and in the normalization of nuclear valence quark distribution (2) (see text for more details).

of the nuclear quark valence number (see Sec. III E). Both approaches give consistent results. We also examined this approach for different nuclei and found similar results for effective cross section at high Q^2 .

For convenience, we provide a parametrization which reasonably fits the numerical solution to the effective cross section for $Q^2 > 4 \text{ GeV}^2$

$$\sigma_T^{\text{eff}}(Q^2) = 0.59 + 18.48 \ln(Q^2/0.37)^{-1.85}, \quad (62)$$

where the cross section is in mb and Q^2 in GeV^2 . In applications discussed in Sec. IV for the cross section, we use Eq.(56) for $Q^2 < 15 \text{ GeV}^2$ and Eq.(62) for higher values of Q^2 .

E. The Gross–Llewellyn-Smith sum rule for nuclei

The Gross–Llewellyn-Smith (GLS) sum is the integrated structure function $F_3^{\nu+\bar{\nu}}$,

$$S_{\text{GLS}}^A = \frac{1}{2} \int_0^{M_A/M} dx F_3^{\nu+\bar{\nu}}(x, Q^2), \quad (63)$$

where we write the GLS sum per one nucleon for a generic nuclear target. In the quark parton model the GLS sum gives the number of valence quarks (baryon number) of the target $S_{\text{GLS}}^A = 3$ [40]. However, in QCD the direct relation between the baryon current and S_{GLS} only holds in the leading twist and leading order in α_s . In contrast to the Adler sum rule, S_{GLS} depends on Q^2 and is affected by QCD radiative corrections, target mass, and the higher-twist effects.

In this section we discuss the GLS integral for nuclear targets. We explicitly separate nuclear corrections to the GLS integral as $S_{\text{GLS}}^A = S_{\text{GLS}}^N + \delta S_{\text{GLS}}$, where S_{GLS}^N refers to the GLS integral for the nucleon (proton). We first consider nuclear corrections to the GLS sum in the LT approximation. The correction due to nuclear binding and Fermi motion cancel out in this

approximation as follows from the direct integration of Eq.(23d) (see also [34]). The nuclear pion correction to $F_3^{\nu+\bar{\nu}}$ also vanishes. However, both, the nuclear shadowing (NS) and the off-shell (OS) corrections to GLS, are generally present. We compute the OS correction to F_3 using Eqs. (28) and (29) and assuming common off-shell function $\delta f_2(x) = \delta f_3(x)$ (see discussion in Sec. III A 2). The NS correction is given by Eq.(50b). We write these corrections for high- Q^2 kinematics and neglect power terms in the structure functions

$$\delta S_{\text{GLS}}^{\text{OS}} = \frac{1}{2} \int_0^1 dx F_{3,\text{LT}}^{(\nu+\bar{\nu})p}(x, Q^2) \delta f(x) \langle v \rangle_0, \quad (64a)$$

$$\delta S_{\text{GLS}}^{\text{NS}} = \frac{1}{2} \int_0^1 dx F_{3,\text{LT}}^{(\nu+\bar{\nu})p}(x, Q^2) \delta \mathcal{R}_T^{(0,-)}(x, Q^2), \quad (64b)$$

where $\langle v \rangle_0 = \langle p^2 - M^2 \rangle_0 / M^2$ is the bound nucleon virtuality averaged with the isoscalar nuclear spectral function \mathcal{P}_0 .

The subscript LT indicates that the structure functions are calculated in the leading twist approximation in QCD. As mentioned above, in LO approximation in α_S , $\frac{1}{2}F_{3,\text{LT}}^{(\nu+\bar{\nu})}$ reduces to the valence quark distribution $u_{\text{val}} + d_{\text{val}}$ and the GLS integral gives the baryon number in the target. For this reason the total nuclear correction to the GLS integral should cancel out. The phenomenological OS and NS corrections driven by Eqs. (30) and (56) indeed largely cancel in the GLS integral, as was shown in Ref.[14] (see Fig. 5 in Ref.[14]). It should be remarked that phenomenological cross section effectively incorporates contributions from all twists since it is extracted from data. Furthermore, at practice the application of Eq.(56) should be limited to $Q^2 < 20 \text{ GeV}^2$ (see also Sec. III D). Higher twists are known to be important at low Q^2 and for this reason we should not expect the exact cancellation between (64a) and (64b) at low Q^2 .

At high Q^2 the LO QCD approximation to structure functions becomes more accurate and the total nuclear correction to the GLS sum rule should cancel out for normalization reason. We evaluate the effective cross section, which provides this cancellation, from the equation $\delta S_{\text{GLS}} = 0$. This equation is solved numerically using the LO approximation for the structure function $x F_3$ and phenomenological off-shell function by Eq.(30).

It should be remarked that the quantity $\delta \mathcal{R}_T^{(0,-)}$, which determines the nuclear shadowing correction to the GSL sum rule, also depends on α_Δ^0 , the Re / Im ratio of the transverse C-odd and isospin 0 effective amplitude [see Eq.(50b)], which is not well known. We assume α_Δ^0 to be independent of energy and Q^2 . In order to fix its value we follow an iterative procedure. In particular, we start from $\alpha_\Delta^0 = 1$, as suggested by simple Regge arguments in Sec. III C 5, and calculate effective cross section $\sigma_T^{\text{eff}}(Q^2)$ from equation $\delta S_{\text{GLS}} = 0$. Then the value of α_Δ^0 is adjusted in order to match $\sigma_T^{\text{eff}}(Q^2)$ at high Q^2 with the cross section calculated from the Adler sum rule in Sec. III D. We found that for $\alpha_\Delta^0 = 1.15$ the two solutions are in a reasonable agreement. The results are shown in Fig. 4 (right panel) together with the results of similar calculation using the Adler sum rule.

IV. NUMERICAL APPLICATIONS

In this section we apply the approach developed in this paper to calculate SFs and cross sections for the targets relevant to recent neutrino scattering experiments. In Sec. IV A we present results for the PCAC contribution to the neutrino SF, in Sec. IV B we discuss the results for heavy nucleus/nucleon ratios of different structure functions, in Sec. IV C we deal

with the numerical analysis of DIS sum rules for nuclear targets, and in Sec. IV D we present our results for nuclear differential cross sections.

A. Low- Q^2 limit

Figure 5 illustrates the magnitude of the PCAC contribution to F_2 for the nucleon and a few nuclear targets calculated by Eq.(22). In this calculation we use the Regge parameterization of πN forward scattering amplitude and the total pion-nucleon cross section of Ref.[31] (see Appendix A). Note that the values of F_2 for heavy nuclear targets are systematically smaller because of the nuclear shadowing effect for the pion cross section (see Sec. III C). In Table II we list the values of F_2 corresponding to the limit $Q^2 \rightarrow 0$ and $x \rightarrow 0$ for the same targets as in Fig. 5. Our results are consistent with the value extracted by the CCFR experiment on an iron target [46].

Target	$\frac{1}{2}(\text{p+n})$	^{12}C	^{56}Fe	^{207}Pb	CCFR (^{56}Fe)
F_2	0.325	0.268	0.235	0.204	0.210 ± 0.02

TABLE II: The value of F_2 in the limit of vanishing Q^2 for neutrino interactions on different targets. The numbers are extracted at $x = 10^{-5}$. The determination from CCFR [46] is also given for comparison.

The PCAC term determines the low- Q^2 limit of F_L , and F_T should vanish as Q^2 in the limit of $Q^2 \rightarrow 0$. In order to describe the structure functions in intermediate region, we apply a smooth interpolation between the high Q^2 regime, which is described in QCD in terms of LT and HT contributions, as discussed in Sec. II C, and the $Q^2 \rightarrow 0$ predictions derived from CVC and PCAC arguments. We use $Q_m^2 = 1 \text{ GeV}^2$ as the matching point between high- and low- Q^2 regimes.

It is instructive to compare the low- Q^2 behavior of $R = F_L/F_T$ for charged-lepton and neutrino scattering. In both cases $F_T \propto Q^2$ as $Q^2 \rightarrow 0$. However, if $F_L \propto Q^4$ for the electromagnetic current, for the weak current $F_L \rightarrow F_L^{\text{PCAC}}$, and thus F_L does not vanish in the low- Q^2 limit. Then the behavior of R at $Q^2 \ll 1 \text{ GeV}^2$ is very different for charged-lepton and neutrino scattering. In order to illustrate this effect we calculate R as a function of Q^2 for two different x (the x -bins of neutrino data [2, 3, 4]) for the isoscalar nucleon and a number of nuclei. The results are shown in Fig. 6.

B. Nuclear structure functions

Figure 7 shows the result of calculation of the C -even structure function $F_2^{\nu+\bar{\nu}}$ of ^{207}Pb . The resulting EMC effect resembles that of CL F_2 (see Ref.[14] for more details). At large x the nuclear correction is driven by FMB and OS effects. We recall that the off-shell effect, which modifies the structure functions of bound nucleon, is important to change the slope of the EMC ratio, bringing it close to data. At intermediate x values we observe some cancellation between the nuclear pion excess and the nuclear shadowing correction. The latter is the dominant effect for $x < 0.05$, providing a suppression of the nuclear structure function.

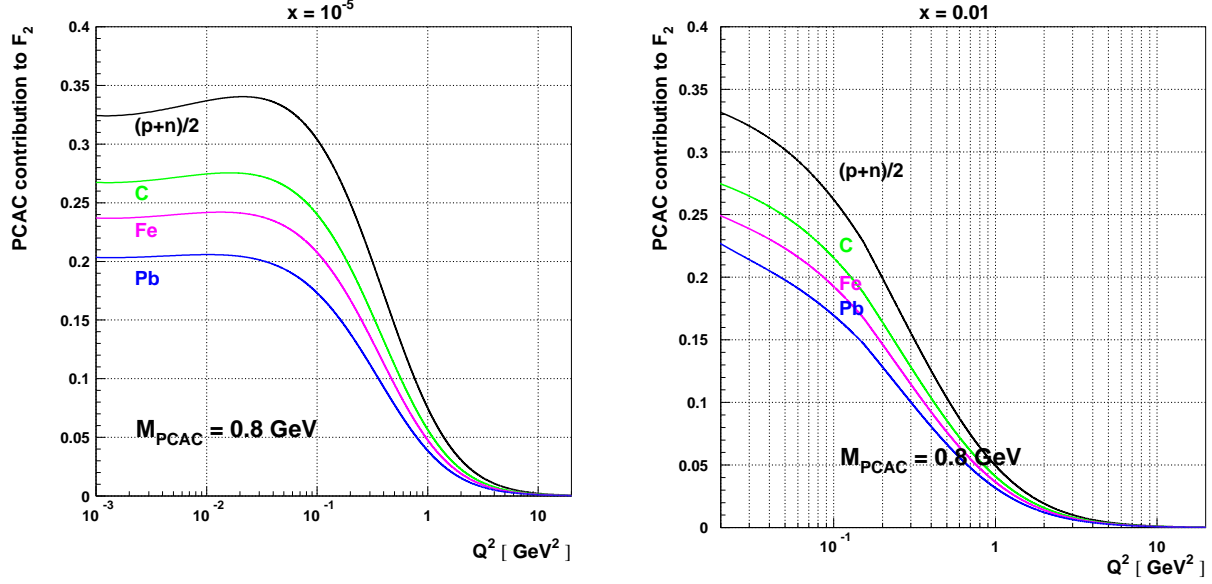


FIG. 5: The PCAC term of the neutrino structure function F_2 (γF_L^{PCAC}) calculated for $x = 10^{-5}$ (left plot) and $x = 10^{-2}$ (right plot) as a function of Q^2 for a few different targets (labels on the curves). A value $M_{\text{PCAC}} = 0.8$ GeV is assumed (see Section IV).

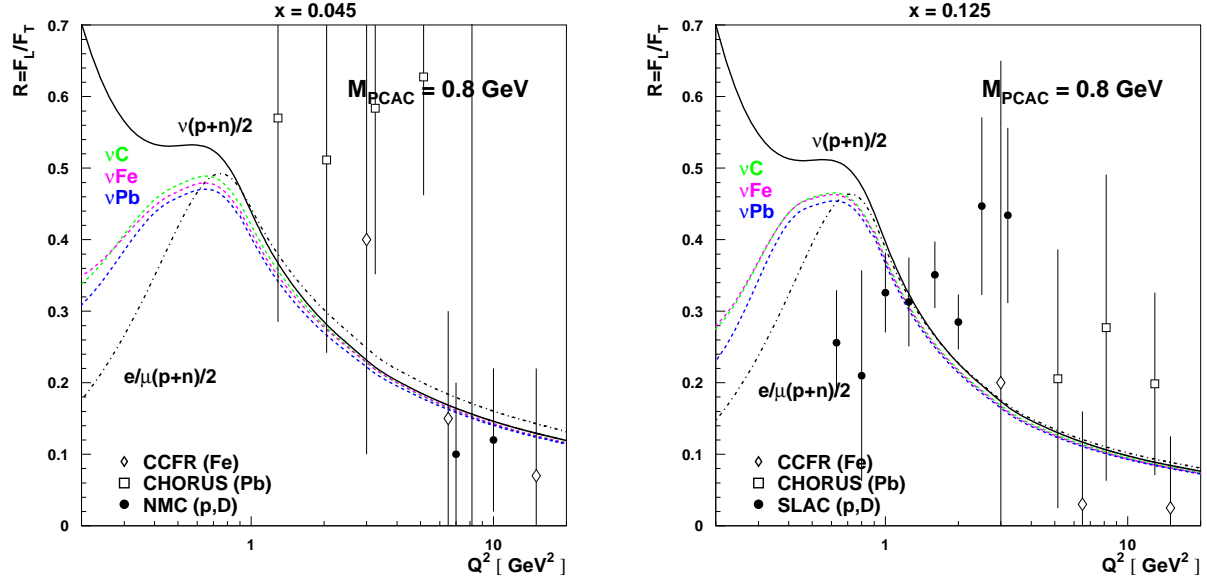


FIG. 6: Comparison of the ratio $R = F_L/F_T$ calculated for the isoscalar nucleon for the charged lepton (dashed-dotted line) and neutrino (solid line) cases at fixed values of x . The left panel corresponds to $x = 0.045$, and the right panel to $x = 0.125$. Also shown are the results for different nuclear targets (^{12}C , ^{56}Fe and ^{207}Pb from top to bottom). A value $M_{\text{PCAC}} = 0.8$ GeV is assumed (see Section IV for more details). Determinations from SLAC [47], CCFR [48] and CHORUS [4] are given for comparison.

The corresponding nuclear corrections for the difference $F_2^{\nu-\bar{\nu}}$ are shown in Fig. 8 after normalizing them to $\beta = (Z - N)/A$. There are two distinct contributions to the difference $F_2^{\nu-\bar{\nu}}$ for nuclear targets [see Eq.(27)]. The pure isovector contribution [second term in Eq.(27)] is shown in Fig. 1. A comparison with Fig. 8 indicates that the dominant contribution to the difference $F_2^{\nu-\bar{\nu}}$ for nuclei is actually coming from the isoscalar part [first term in Eq.(27)], which is due to the Cabibbo mixing and the heavy quark production effects.

It must be also noted that coherent nuclear effects are particularly pronounced in the C -odd channel, as can be seen from Fig. 8 (the shadowing effect at small x). The antishadowing effect at $x \sim 0.05$ is a combined effect due to nuclear smearing (FMB) and a constructive interference in the coherent nuclear correction due to the real part of the effective amplitude.

Using the approach described in previous sections we calculate the ratios $\mathcal{R}_2^\nu = F_2^{\nu A}/F_2^{\nu(p+n)/2}$ and $\mathcal{R}_3^\nu = F_3^{\nu A}/F_3^{\nu(p+n)/2}$ for CC neutrino interactions for the Fe and Pb targets. The results are shown in Fig. 9. The bulk behavior of \mathcal{R}_2^ν is similar to that of \mathcal{R}_2^μ in CL scattering (see [14]) for both the x and Q^2 dependencies. Note that for heavy nuclei with an excess of neutrons over protons $\mathcal{R}_2^\nu > \mathcal{R}_2^\mu$ for $x > 0.1$. This is because the neutron excess correction is positive for the neutrino case, while this correction is negative for CL scattering. Indeed, this correction is given by the second term in Eq.(25). Because $F_2^{\mu(p-n)} > 0$ and $F_2^{\nu(p-n)} < 0$, we obtain the different sign of the neutron excess correction in these cases. It should be also remarked that this correction is negative for antineutrino SFs, similar to the CL case. As a result there is a cancellation for the neutron excess correction in the sum $F_2^{\nu+\bar{\nu}}$, as can be seen in Fig. 7. It is interesting to note that in the antineutrino case different nuclear effects cancel to a high degree in the region $x \sim 0.1$ (see also Fig. 11).

It is also instructive to compare nuclear effects for neutrino SFs F_2 and xF_3 . One observes from Fig. 9 that at large Q^2 ($= 10 \text{ GeV}^2$) the ratios \mathcal{R}_2^ν and \mathcal{R}_3^ν turn out to be similar (although not identical) in the entire kinematical region of x . We recall in this context that the effect of coherent nuclear interactions at small x is quite different for F_2 and xF_3 (see Sec. III C). Furthermore, the nuclear pion correction to xF_3 cancels out, and the antishadowing effect for F_2 and xF_3 is generated by different mechanisms (the combined effect of the real part of the C -odd effective amplitude and the off-shell correction for xF_3 and the interplay between pion and off-shell effect for F_2). Nevertheless, at high Q^2 the total nuclear correction to xF_3 is very similar to that for F_2 .

The differences between \mathcal{R}_2 and \mathcal{R}_3 are more pronounced at lower Q^2 , indicating different Q^2 dependence of nuclear effects for these structure functions. The shadowing and antishadowing effects for F_3 become stronger in this region as illustrated in Fig. 9.

Also one should remark that the target mass correction to the structure functions strongly affects the EMC ratio in the region of large x and low $Q^2 \sim 1 \text{ GeV}^2$. This effect causes a noticeable Q^2 dependence of the EMC ratio at $x > 0.6$. We also note that in Fig. 9 the curves for $Q^2 = 1 \text{ GeV}^2$ are given for the region $W > 1.25 \text{ GeV}$ and for this reason the region $x > 0.6$ is not shown.

C. Neutrino DIS sum rules

As discussed in Sections III D and III E, we observe a remarkable cancellation between the off-shell and the nuclear shadowing corrections. This cancellation, which becomes more accurate at high Q^2 where the leading twist dominates, can be attributed to underlying symmetry through the conservation of the isospin (Adler) and the nuclear valence quark

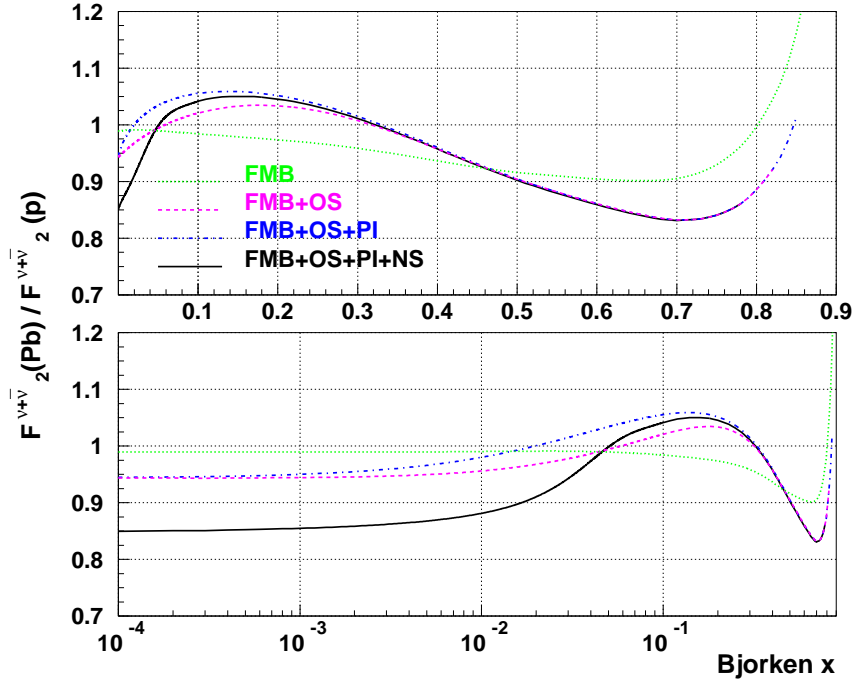


FIG. 7: Different nuclear effects on the ratio $\frac{1}{A}F_2^{(\nu+\bar{\nu})A}/F_2^{(\nu+\bar{\nu})p}$ calculated for ^{207}Pb at $Q^2 = 5 \text{ GeV}^2$. The labels on the curves correspond to effects due to Fermi motion and nuclear binding (FMB), off-shell correction (OS), nuclear pion excess (PI) and coherent nuclear processes (NS).

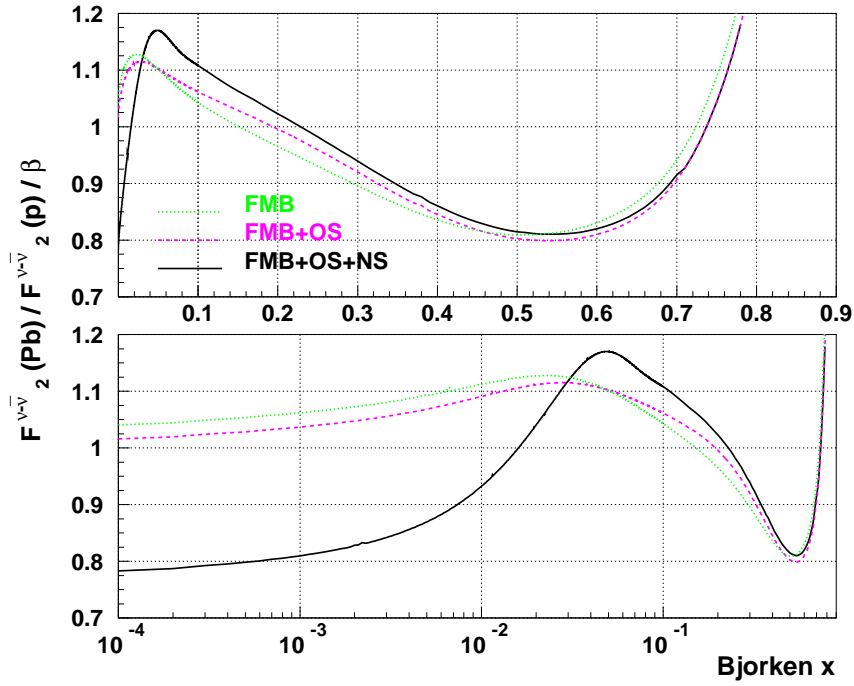


FIG. 8: Different nuclear effects on the ratio $\frac{1}{A}F_2^{(\nu-\bar{\nu})A}/(\beta F_2^{(\nu-\bar{\nu})p})$ calculated for ^{207}Pb at $Q^2 = 5 \text{ GeV}^2$. The labels on the curves correspond to effects due to Fermi motion and nuclear binding (FMB), off-shell correction (OS) and coherent nuclear processes (NS).

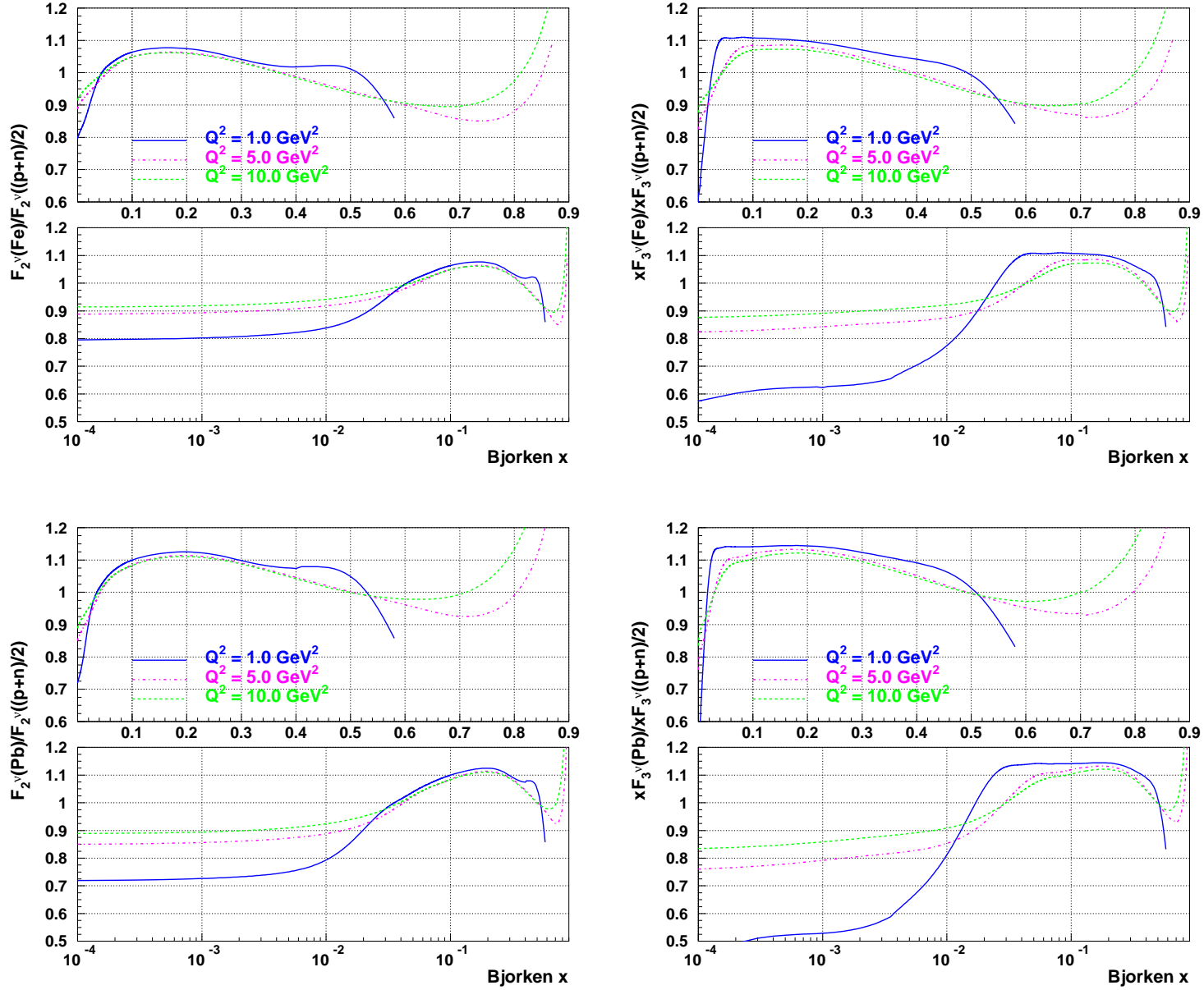


FIG. 9: Our predictions for the ratios of CC neutrino nuclear structure functions normalized to one nucleon and those of the isoscalar nucleon $(p+n)/2$ (left panel for F_2 and right panel for xF_3). The ratios were calculated for ^{56}Fe (upper panels) and ^{207}Pb (lower panels) as a function of x at $Q^2 = 1, 5, \text{ and } 10 \text{ GeV}^2$.

number (GLS) in nuclear targets. Assuming exact cancellation we evaluate the effective cross-section describing the nuclear shadowing at high- Q^2 . Both the Adler and GLS sum rules can be used for this purpose, providing consistent results. In this paper we choose the Adler integral since the corresponding isospin relation is accurate to all orders. Furthermore, the evaluation of the Adler sum rule for nuclear targets involves the off-shell function δf_2 , which was determined from charged-lepton DIS data.

We can then evaluate the GLS integral $S_{\text{GLS}}(Q^2)$ for different nuclear targets. Results are shown in Fig. 10. The nucleon integral $S_{\text{GLS}}^N(Q^2)$ is calculated using the NNLO coefficient functions and the NNLO PDFs of [24]. We observe that the nuclear correction δS_{GLS} decreases progressively by increasing Q^2 and ranges from about 2% at $Q^2 = 2 \text{ GeV}^2$ to less than 0.3% at $Q^2 = 20 \text{ GeV}^2$. The results for different targets are similar and noticeable differences are present only at the lowest Q^2 values. We also note the general Q^2 dependence for ^{56}Fe is in agreement with the CCFR measurement [41]. The values of S_{GLS}^N and δS_{GLS} are listed in Table III for a number of nuclear targets and fixed value of $Q^2 = 10 \text{ GeV}^2$.

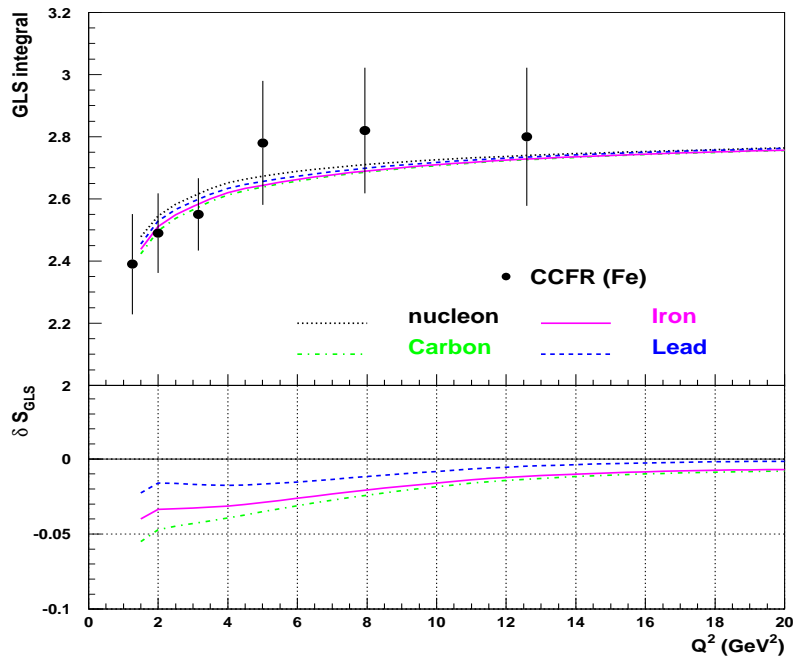


FIG. 10: The GLS integral for different nuclear targets as a function of Q^2 . The nucleon $x F_3$ is calculated in LT NNLO approximation with the target mass correction as described in Sec. II C. The bottom panel shows variations with respect to the result obtained for average isoscalar nucleon. Data points are the CCFR extraction of the GLS integral for iron [41].

Power corrections due to target mass effect are included in the calculation. Apart from the target mass effect the dynamical power corrections should generally be present. The contribution of such terms to the GLS integral was evaluated in [42] using QCD sum rule approach, predicting a negative correction of -0.1 at $Q^2 = 3 \text{ GeV}^2$. We also comment that phenomenological studies of HT terms in F_3 using CCFR data were reported in [25] with, however, high statistical uncertainties. In this context we note the current analysis of combined (anti)neutrino cross-section data [26] that would allow to greatly reduce statistical uncertainty in the neutrino HT terms.

Target	Comment	S_{GLS}	δS_{GLS}
p	free proton	2.726	0
D	full calculation	2.717	-0.009
^{12}C	full calculation	2.707	-0.019
^{56}Fe	full calculation	2.710	-0.016
^{207}Pb	full calculation	2.717	-0.009

TABLE III: The GLS sum rule calculated for different nuclei at $Q^2 = 10 \text{ GeV}^2$. The nucleon structure functions were calculated in LT NNLO approximation using the PDFs of Ref.[24]. We use the lower cutoff $x_{\text{min}} = 10^{-5}$ in the calculation of the GLS integral.

The nuclear effects somewhat modify the Q^2 evolution of the GLS integral. This is mainly due to the explicit Q^2 dependence of effective cross section describing the nuclear shadowing effect. As can be seen from Fig. 10 the correction is negative and of the order of 2% at low Q^2 . This must be compared with the variation related to the running α_s , which is about 10% between 2 and 20 GeV^2 . Nuclear corrections should be then taken into account for precise extractions of α_s from the GLS sum rule (see also [43]). The effect of nuclear corrections would indeed reduce the measured value of the strong coupling constant, by reducing the Q^2 slope in the GLS integral.

D. Comparison with cross section data

Using the results on nuclear structure functions we calculate the neutrino and antineutrino inelastic inclusive differential cross-sections. Figure 11 summarizes our results for the corresponding nuclear dependence. We note a cancellation between different nuclear effects for antineutrino at $x \sim 0.1 \div 0.2$. As a result, the antineutrino cross section is not very sensitive to the target material in this region. Note also the cancellation of nuclear effects for $x \sim 0.3$ for the isoscalar target (^{12}C). Nuclear effect in this region is driven by the neutron excess.

We can then compare our predictions with the available data on differential cross sections for different targets. Table IV summarizes the most recent and precise measurements on ^{12}C (NOMAD), ^{56}Fe (NuTeV) and ^{207}Pb (CHORUS).⁷ It must be noted that when comparing with data the predictions have to include electroweak (EW) corrections related to virtual loop diagrams, soft photon emission and hard photon emission. The effect of such processes is to shift the measured kinematic variables and hence to modify the differential cross sections. To this end, in this paper we use the recent one-loop calculations of Ref. [44] (see also Ref. [45]). We also implicitly assume that EW and nuclear corrections factorize so that they can be applied to the final nuclear structure functions.⁸

In Figs. 12 to 14 we report the comparisons between measurements and our calculations for several values of the (anti)neutrino energy ranging from 20 GeV to 170 GeV. In this

⁷ We use the cross-section data for all our studies and not structure function data provided by experiments. This procedure minimizes potential biases related to different model assumptions used in extractions of structure functions by individual experiments.

⁸ We note that the magnitude of EW corrections in some specific kinematic regions can be comparable with nuclear corrections.

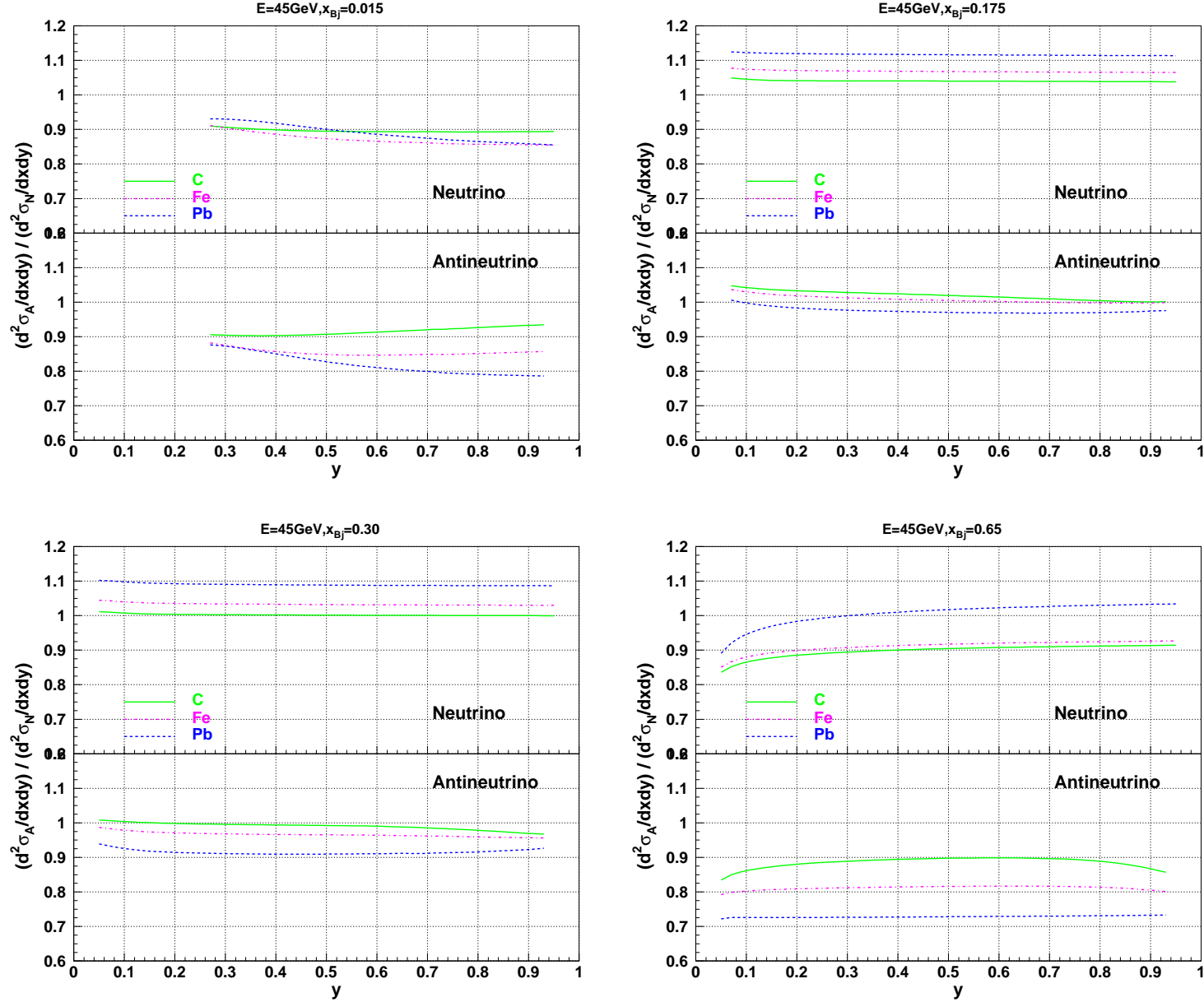


FIG. 11: The ratio of (anti)neutrino nuclear and the isoscalar nucleon differential cross sections calculated for ^{12}C , ^{56}Fe and ^{207}Pb targets at $E = 45$ GeV. The electroweak correction is taken into account using Ref.[44].

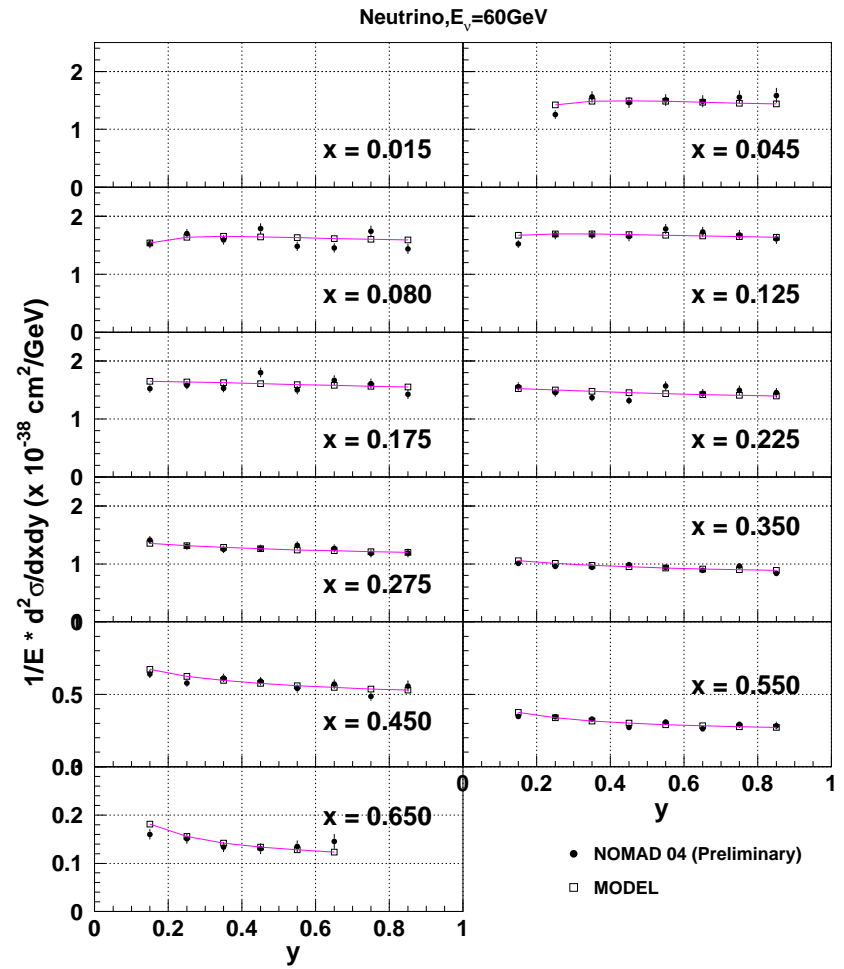
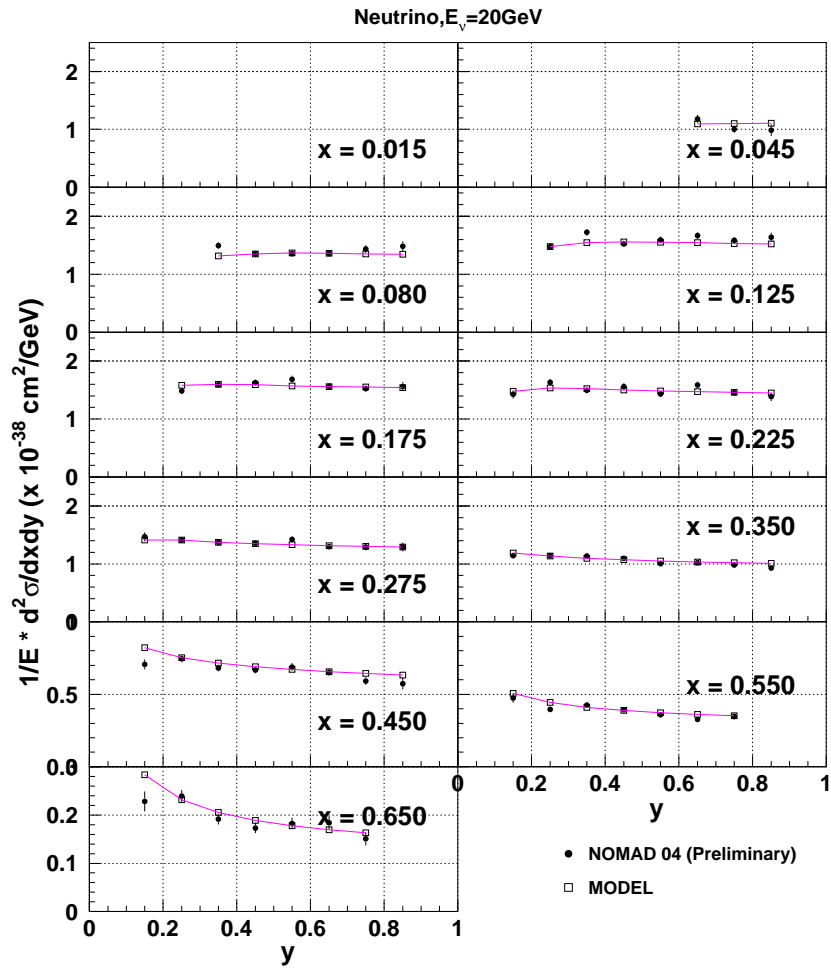


FIG. 12: Comparison of our predictions (open symbols) with NOMAD data (full symbols) for neutrino differential cross-sections on ^{12}C at $E = 20 \text{ GeV}$ (left plot) and $E = 60 \text{ GeV}$ (right plot). See text for details.

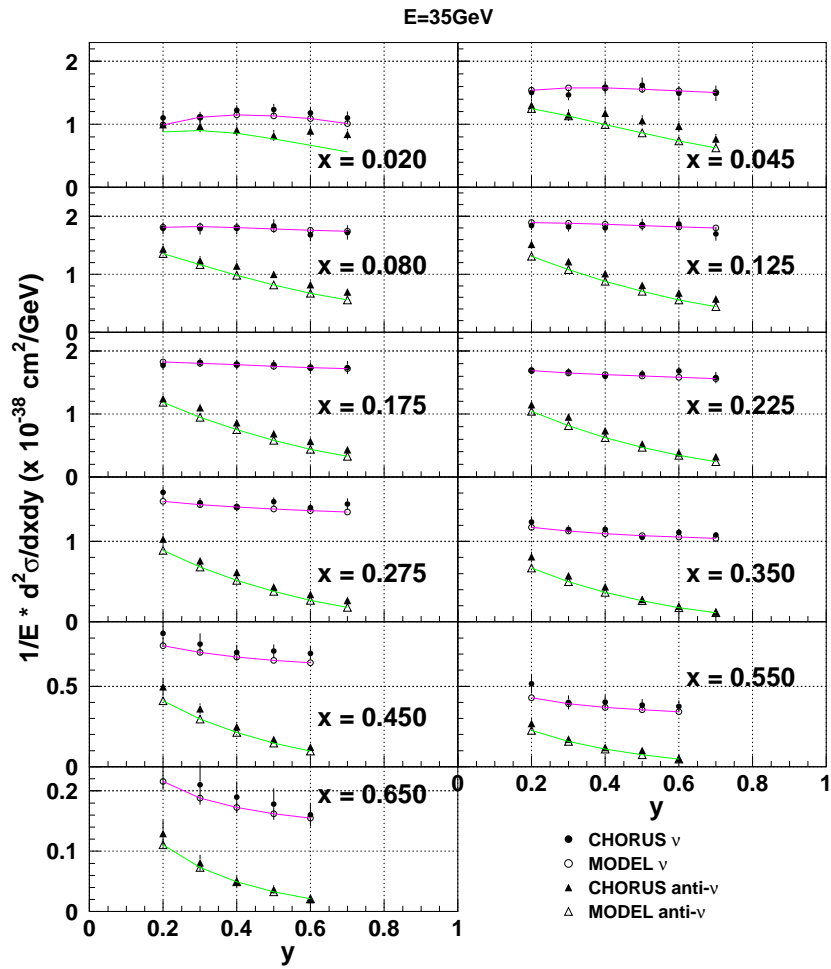


FIG. 13: Comparison of our predictions (open symbols) with CHORUS data (full symbols) for neutrino (circles) and antineutrino (triangles) differential cross-sections on ^{207}Pb at $E = 35$ GeV (left plot) and $E = 90$ GeV (right plot). See text for details.

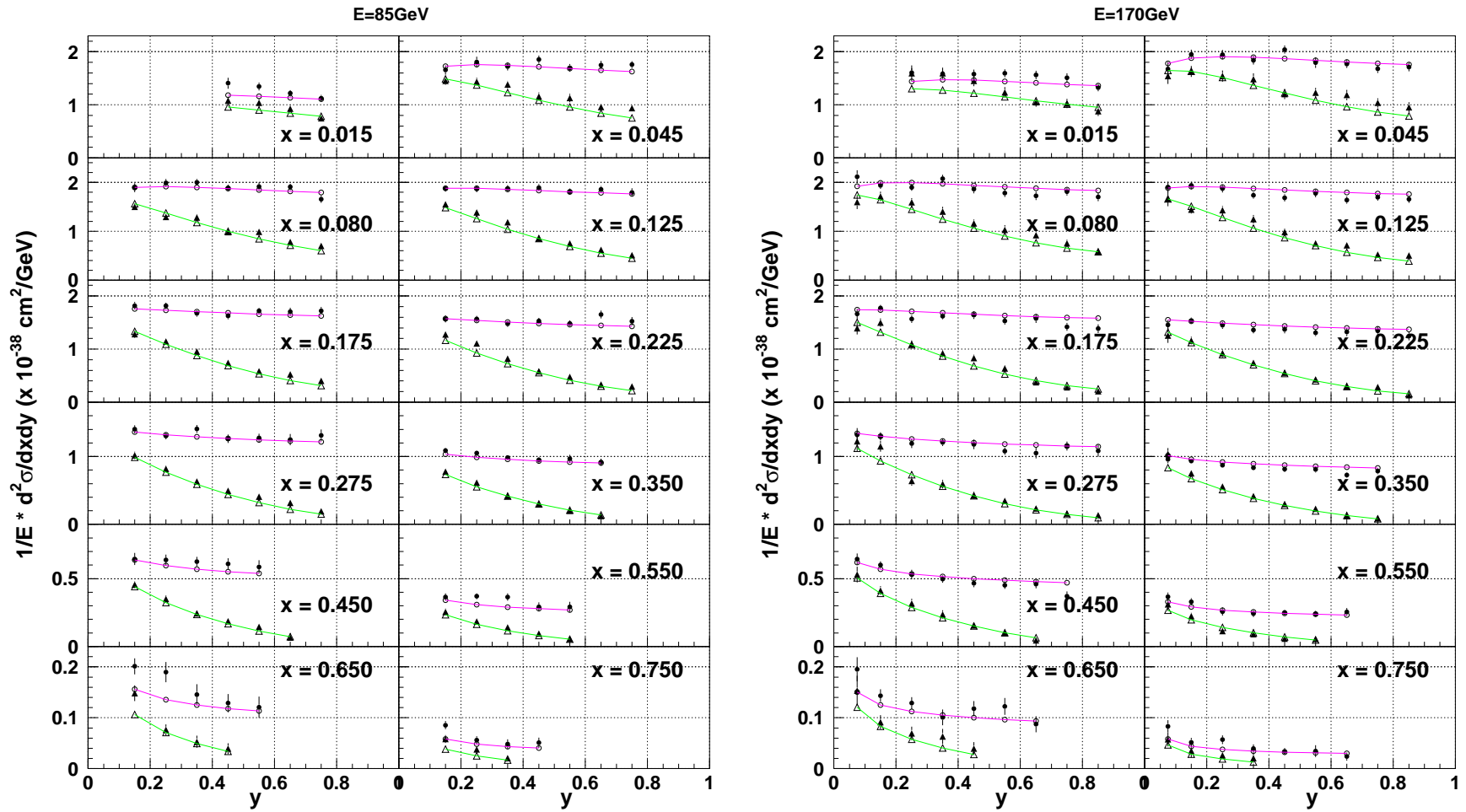


FIG. 14: Comparison of our predictions (open symbols) with NuTeV data (full symbols) for neutrino (circles) and antineutrino (triangles) differential cross-sections on ^{56}Fe at $E = 85 \text{ GeV}$ (left plot) and $E = 170 \text{ GeV}$ (right plot). See text for details.

Experiment	Beam	Target	Statistics	E values [GeV]	x values	y values	Number of points
NOMAD[3]	ν	^{12}C	750k	20÷200	0.015÷0.65	0.15÷0.85	563
NuTeV[2]	ν	^{56}Fe	860k	35÷340	0.015÷0.75	0.05÷0.95	1423
	$\bar{\nu}$	^{56}Fe	240k	35÷340	0.015÷0.75	0.05÷0.85	1195
CHORUS[4]	ν	^{207}Pb	930k	25÷170	0.020÷0.65	0.10÷0.80	607
	$\bar{\nu}$	^{207}Pb	160k	25÷170	0.020÷0.65	0.10÷0.80	607

TABLE IV: The list of neutrino and antineutrino data samples (after analysis cuts) corresponding to the cross-section measurements used in this paper.

calculations we use both the nucleon parton distributions and the HT terms obtained from the fits to charged-lepton DIS data [24]. In the presented results the LT structure functions were evaluated in the NNLO approximation. In order to evaluate the HT contribution to neutrino structure functions F_2 and F_T we use the phenomenological charged-lepton HT terms rescaled according to the corresponding ratio of neutrino to the CL structure function in the LT approximation. No HT contribution is included for $x F_3$. A more detailed study of (anti)neutrino data in the context of QCD fits and of the extraction of HT terms will be published elsewhere [26]. Note that the approach discussed was successfully applied in the analysis of charged-lepton nuclear data (the nuclear EMC effect) [14]. The comparison with neutrino data provides an independent verification of our model and also allows a compatibility check between (anti)neutrinos and charged leptons.

In general, we observe good agreement between data and our predictions for all nuclei. We note that this also includes the lowest Q^2 data points, which in the case of CHORUS are at $Q^2 \sim 0.25 \text{ GeV}^2$. The Q^2 dependence in the low x bins is also reproduced, as can be seen from the y distributions and by comparing different (anti)neutrino energies. The existing cross-section data in the low x and low Q^2 region support the presence of the PCAC term in the longitudinal structure function. A value of the scale $M_{\text{PCAC}} = 0.8 \text{ GeV}$ seems to provide the best agreement with data.

After verifying the consistency of our cross-section model with (anti)neutrino data, it is interesting to use the model to examine the compatibility of data from different experiments and nuclear targets. At small and intermediate values of x the three experiments are in agreement for both the neutrino and antineutrino samples. At large values of $x > 0.45$ the NuTeV data seem to be systematically above calculations for most neutrino energies. On the other hand, the corresponding predictions for ^{12}C and ^{207}Pb at large x are in agreement with NOMAD and CHORUS data, respectively.

The low- Q^2 and low- x behaviour of the (anti)neutrino cross section is dominated by the divergence of the axial current and PCAC relation. However, as discussed in Section IID, the scale controlling the PCAC contribution to the longitudinal structure function is not well known. The use of heavy targets introduces additional uncertainties. The MINER ν A experiment [9], recently proposed at Fermilab and currently under construction, has the possibility to address PCAC effect (as well as other nuclear effects) in heavy nuclei. To this end, the possibility to have cryogenic hydrogen and deuterium targets would greatly enhance the corresponding physics potential.

V. SUMMARY

We discussed inelastic inclusive scattering of high-energy (anti)neutrino off nuclei and developed a quantitative model for nuclear structure functions using an approach which takes into account the QCD treatment of the nucleon structure functions and addresses the basic nuclear effects including nuclear shadowing, Fermi motion and nuclear binding, nuclear pions and off-shell corrections to bound nucleon structure functions.

The presence of both the axial and the vector currents in neutrino interactions results in contributions with different C -parity to neutrino cross sections. The interference between the vector and the axial current is described by the structure function F_3 which is not present in charged-lepton scattering. We discussed in detail how the nuclear effects depend on the structure function type (F_2 vs xF_3) and on the C -parity of structure functions (C -even $\nu + \bar{\nu}$ and C -odd $\nu - \bar{\nu}$ combinations).

The axial-vector current plays a special role in neutrino scattering in the region of low Q^2 and low x . In this region the cross sections are dominated by contributions from the divergence of the axial current which is linked to the virtual pion cross section via the Adler relation. Using PCAC we examined the derivation of low Q^2 and low x limit for neutrino structure functions and discussed the scale in Q^2 at which the Adler relation can be applied. We studied this problem phenomenologically using low- Q^2 and low- x neutrino cross-section data.

We examined the Adler and the Gross–Llewellyn-Smith sum rules for nuclear structure functions. A remarkable cancellation between nuclear shadowing and off-shell corrections was found, underlying the conservation of isospin and valence quark number in nuclei. This fact was used to constrain the effective scattering amplitude controlling the nuclear shadowing for different C -parity and isospin states.

We applied our results to calculate nuclear structure functions for the targets and kinematical conditions typical for recent neutrino experiments. Our predictions for the (anti)neutrino inelastic differential cross-sections agree well with the recent data on ^{12}C [3], ^{56}Fe [2], and ^{207}Pb [4].

We conclude by commenting that the nuclear corrections prove to be particularly important for QCD phenomenology of $\nu(\bar{\nu})$ data on heavy targets, where they significantly affect the fit results [26].

Acknowledgments

We thank S. Alekhin, A. Butkevich, A. Kataev, and S. Mishra for useful discussions and comments, J. Panman for providing the tables of CHORUS cross-section data, M. Tzanov for useful information about the NuTeV cross sections, and the NOMAD Collaboration for the use of their preliminary data. S.K. was partially supported by Russian Foundation for Basic Research Project No. 06-02-16659 and 06-02-16353 and by INTAS Project No. 03-51-4007. R.P. thanks USC for supporting this research.

APPENDIX A: PARAMETERIZATION OF THE PION–NUCLEON SCATTERING AMPLITUDE

The parametrization of the pion–nucleon forward scattering amplitude based on a Regge fit to πN scattering data is given in Ref.[31]:

$$a_{\pi^{\pm}p} = a_{\pi}^0 \pm \frac{1}{2}a_{\pi}^1, \quad (\text{A1})$$

$$a_{\pi}^0(s) = \frac{X}{2}s^{\epsilon} \left[i - \cot \left(\frac{\pi}{2}(1 + \epsilon) \right) \right] + \frac{Y_1}{2}s^{-\eta_1} \left[i - \cot \left(\frac{\pi}{2}(1 - \eta_1) \right) \right], \quad (\text{A2})$$

$$a_{\pi}^1(s) = -Y_2s^{-\eta_2} \left[i + \tan \left(\frac{\pi}{2}(1 - \eta_2) \right) \right]. \quad (\text{A3})$$

In Eq.(A1) the amplitude $a_{\pi}^{0(1)}$ corresponds to the pion coupling to the isoscalar (isovector) nucleon configuration and the sign $+(-)$ corresponds to the $\pi^+(\pi^-)$ meson. The pion-neutron scattering amplitude is derived from isospin relations $a_{\pi^{\pm}n} = a_{\pi^{\mp}p}$. The parameters are

$$X = 12.08 \pm 0.29, \quad \epsilon = 0.0933 \pm 0.0024, \quad (\text{A4})$$

$$Y_1 = 26.2 \pm 0.74, \quad \eta_1 = 0.357 \pm 0.015, \quad (\text{A5})$$

$$Y_2 = 0.560 \pm 0.017, \quad \eta_2 = 0.560 \pm 0.017. \quad (\text{A6})$$

We also note that the forward scattering amplitude is normalized as $\text{Im} a_{\pi} = \sigma_{\pi}/2$ with σ_{π} the total cross section, and the units of the parameters X and $Y_{1,2}$ are such that a_{π} is measured in mb if s is in GeV^2 .

-
- [1] “NuInt05, proceedings of the 4th International Workshop on Neutrino-Nucleus Interactions in the Few-GeV Region, Okayama, Japan, 26-29 September 2005”, F. Cavanna, J. G. Morfin and T. Nakaya, Eds., Nucl. Phys. Proc. Suppl. **159** (2006).
- [2] M. Tzanov [NuTeV Collaboration], arXiv:hep-ex/0507040.
- [3] R. Petti [NOMAD Collaboration], arXiv:hep-ex/0602022.
- [4] G. Önençüt *et al.*[CHORUS Collaboration], Phys. Lett. B. **632**, 65 (2006).
- [5] G. A. Miller and A. W. Thomas, arXiv:hep-ex/0204007; S. Kovalenko *et al.*, Phys. Lett. B **546**, 68 (2002) [arXiv:hep-ph/0207158]; S. Kumano, Phys. Rev. D **66**, 111301 (2002) [arXiv:hep-ph/0209200]; M. Hirai *et al.*, Phys. Rev. C **70**, 044905 (2004) [arXiv:hep-ph/0404093]; S. A. Kulagin, Phys. Rev. D **67**, 091301 (2003) [arXiv:hep-ph/0301045]; S. A. Kulagin, arXiv:hep-ph/0406220. S. J. Brodsky *et al.*, Phys. Rev. D **70**, 116003 (2004) [arXiv:hep-ph/0409279].
- [6] G. P. Zeller *et al.*, Phys. Rev. Lett. **88**, 091802 (2002) [arXiv:hep-ex/0110059].
- [7] J. Hylen *et al.*, Fermilab Report No. TM-2018 (1997); L. Bartoszek *et al.*, arXiv:hep-ex/0408121;
- [8] Japan Proton Accelerator Research Complex, <http://jkj.tokai.jaeri.go.jp/>.
- [9] D. Drakoulakos *et al.* [Minerva Collaboration], arXiv:hep-ex/0405002.
- [10] M. L. Mangano *et al.*, arXiv:hep-ph/0105155; A. Blondel *et al.*, CERN-2004-002; M. M. Alsharoa *et al.* [Muon Collider/Neutrino Factory Collaboration], Phys. Rev. ST Accel. Beams **6**, 081001 (2003) [arXiv:hep-ex/0207031].

- [11] M. Arneodo, Phys. Rept. **240**, 301 (1994).
- [12] G. Piller and W. Weise, Phys. Rept. **330**, 1 (2000) [arXiv:hep-ph/9908230].
- [13] D. F. Geesaman, K. Saito, and A. W. Thomas, Annu. Rev. Nucl. Part. Sci. **45** 337 (1995).
- [14] S. A. Kulagin and R. Petti, Nucl. Phys. A **765**, 126 (2006) [arXiv:hep-ph/0412425].
- [15] S. L. Adler, Phys. Rev. **135**, B963 (1964).
- [16] B. L. Ioffe, V. A. Khoze and L. N. Lipatov, *Hard Processes. Vol. 1: Phenomenology, Quark-Parton Model*, (North-Holland Physics Publishing, Amsterdam, 1984).
- [17] K. G. Wilson, Phys. Rev. **179**, 1499 (1969); E. V. Shuryak and A. I. Vainshtein, Nucl. Phys. B **199**, 451 (1982).
- [18] R. Brock *et al.* [CTEQ Collaboration], Rev. Mod. Phys. **67**, 157 (1995).
- [19] L. N. Lipatov, Sov. J. Nucl. Phys. **20**, 94 (1975) [Yad. Fiz. **20**, 181 (1974)]; G. Altarelli and G. Parisi, Nucl. Phys. B **126**, 298 (1977); Y. L. Dokshitzer, Sov. Phys. JETP **46**, 641 (1977) [Zh. Eksp. Teor. Fiz. **73**, 1216 (1977)].
- [20] W. L. van Neerven and E. B. Zijlstra, Phys. Lett. B **272**, 127 (1991); E. B. Zijlstra and W. L. van Neerven, Nucl. Phys. B **383**, 525 (1992).
- [21] S. Moch, J. A. M. Vermaseren and A. Vogt, Nucl. Phys. B **688**, 101 (2004) [arXiv:hep-ph/0403192]; A. Vogt, S. Moch and J. A. M. Vermaseren, Nucl. Phys. B **691**, 129 (2004) [arXiv:hep-ph/0404111].
- [22] H. Georgi and H. D. Politzer, Phys. Rev. D **14**, 1829 (1976).
- [23] O. Nachtmann, Nucl. Phys. B **63**, 237 (1973).
- [24] S. Alekhin, Phys. Rev. D **68**, 014002 (2003); S. Alekhin, K. Melnikov, and F. Petriello, Phys. Rev. D **74**, 054033 (2006).
- [25] A. L. Kataev, G. Parente and A. V. Sidorov, Nucl. Phys. B **573**, 405 (2000) [arXiv:hep-ph/9905310]; Phys. Part. Nucl. **34**, 20 (2003) [Fiz. Elem. Chast. Atom. Yadra **34**, 43 (2003)] [arXiv:hep-ph/0106221].
- [26] S. Alekhin, S. A. Kulagin and R. Petti, arXiv:0710.0124 [hep-ph].
- [27] C. H. Albright and C. Jarlskog, Nucl. Phys. B **84**, 467 (1975).
- [28] S. Kretzer and M. H. Reno, Phys. Rev. D **66**, 113007 (2002) [arXiv:hep-ph/0208187].
- [29] B. Z. Kopeliovich and P. Marage, Int. J. Mod. Phys. A **8**, 1513 (1993); B. Z. Kopeliovich, Nucl. Phys. Proc. Suppl. **139**, 219 (2005) [arXiv:hep-ph/0409079].
- [30] G. T. Jones *et al.*, Z. Phys. C **37**, 25 (1987).
- [31] J. R. Cudell *et al.*, Phys. Rev. D **61**, 034019 (2000) [Erratum-ibid. D **63**, 059901 (2001)] [arXiv:hep-ph/9908218].
- [32] S. A. Kulagin, Nucl. Phys. A **500**, 653 (1989).
- [33] S. A. Kulagin, G. Piller and W. Weise, Phys. Rev. C **50**, 1154 (1994) [arXiv:nucl-th/9402015].
- [34] S. A. Kulagin, Nucl. Phys. A **640**, 435 (1998) [arXiv:nucl-th/9801039].
- [35] R. J. Glauber, Phys. Rev. **100**, 242 (1955).
- [36] V. N. Gribov, Sov. Phys. JETP **30**, 709 (1970) [Zh. Eksp. Teor. Fiz. **57**, 1306 (1969)].
- [37] T. H. Bauer, R. D. Spital, D. R. Yennie and F. M. Pipkin, Rev. Mod. Phys. **50**, 261 (1978) [Erratum-ibid. **51**, 407 (1979)]; C. A. Piketty and L. Stodolsky, Nucl. Phys. B **15**, 571 (1970).
- [38] S. A. Kulagin, arXiv:hep-ph/9812532.
- [39] P. D. B. Collins, *An Introduction To Regge Theory And High-Energy Physics* (Cambridge Univ. Press, Cambridge, 1977).
- [40] D. J. Gross and C. H. Llewellyn Smith, Nucl. Phys. B **14**, 337 (1969).
- [41] J. H. Kim *et al.*, Phys. Rev. Lett. **81** (1998) 3595 [arXiv:hep-ex/9808015].
- [42] V. M. Braun and A. V. Kolesnichenko, Nucl. Phys. B **283**, 723 (1987).

- [43] S. A. Kulagin and A. V. Sidorov, Eur. Phys. J. A **9**, 261 (2000) [arXiv:hep-ph/0009150].
- [44] A. B. Arbuzov, D. Y. Bardin and L. V. Kalinovskaya, JHEP **0506**, 078 (2005) [arXiv:hep-ph/0407203].
- [45] K. P. Diener, S. Dittmaier and W. Hollik, Phys. Rev. D **69**, 073005 (2004).
- [46] B. T. Fleming *et al.* [CCFR Collaboration], Phys. Rev. Lett. **86**, 5430 (2001).
- [47] L. W. Whitlow *et al.*, Phys. Lett. B **250**, 193 (1990).
- [48] U. K. Yang *et al.* [CCFR/NuTeV Collaboration], Phys. Rev. Lett. **87**, 251802 (2001).